

A SURVEY OF FINITE-DIFFERENCE SCHEMES FOR THE PRIMITIVE EQUATIONS FOR A BAROTROPIC FLUID

ARNE GRAMMELTVEDT¹

National Center for Atmospheric Research, Boulder, Colo.²

ABSTRACT

Ten different finite-difference schemes for the numerical integration of the primitive equations for the free-surface model are tested for stability and accuracy. The integrations show that the quadratic conservative and the total energy conservative schemes are more stable than the usual second-order conservative scheme. But the most stable schemes are those in which the finite-difference approximations to the advection terms are calculated over nine grid points in space and therefore contain a form of smoothing, and the generalized Arakawa scheme, which for nondivergent flow conserve mean vorticity, mean kinetic energy, and mean square vorticity.

If the integrations are performed for more than 3 days, it is shown that more than 15 grid points per wavelength are probably needed to describe with accuracy the movement and development of the shortest wave that initially is carrying a significant part of the energy. This is true even if a fourth-order scheme in space is used.

Long-term integrations using the leapfrog method or midpoint rule in time may lead to instability of the integration from the increase of energy on the computational modes. Elimination of the computational modes by using a smoothing operator in time or by using other multistep time-integration methods, which damp the computational modes, will improve the stability of the integration.

As a rule, linear stable one-step methods have strong built-in dissipation and in a few days will damp out most of the initial perturbation energy, even if they are used only intermittently once a day.

1. INTRODUCTION

Numerical integration of the nonlinear initial value problems in fluid dynamics and meteorology may introduce computational instability from the finite-difference approximation to the nonlinear terms of the equations. This instability, caused by the finite number of waves that can be resolved in a grid and that cannot be suppressed by using a shorter time step, was first demonstrated for the vorticity equation describing two-dimensional incompressible flow by Phillips (1959); Miyakoda (1962) showed that this type of instability may also occur for the linear equations with variable coefficients. The most commonly used methods to suppress this instability are to introduce artificial viscosity terms in the finite-difference equations or to write the finite-difference equations in a form that conserves certain statistical moments of the dependent variables.

An artificial viscosity term was first introduced by von Neumann and Richtmyer (1950) in numerical calculations of hydrodynamic shocks. They added a nonlinear viscosity term to the finite-difference equation to enlarge the shock zone. Artificial viscosity is also incorporated in the finite-difference formulation of Lax and Wendroff (1960) and has been used by Houghton, Kasahara, and Washington (1966) in long-term integration of the equations describing barotropic flow with a free surface. The same barotropic equations are also integrated by Shuman and Vanderman (1966). They use finite-

difference approximations to the advection terms, which are calculated over nine grid points in space; and a form of smoothing is, therefore, introduced into the finite-difference equations.

For the vorticity equation describing two-dimensional incompressible flow, Arakawa (1966) has developed spatial finite-difference equations that are nonlinearly computationally stable by retaining in the finite-difference equations some of the integral properties of the continuous equation, namely the integral of vorticity, kinetic energy, and square of vorticity. But, as pointed out by Arakawa, only one of these quadratic conservative properties is necessary for the solution to be nonlinearly stable. Using the same principles, Lilly (1965) has developed a general spatial momentum and total energy conservative finite-difference scheme for the nonlinear terms in the two-dimensional barotropic equations. This general momentum and energy-conserving representation of the nonlinear terms is used by Smagorinsky, Manabe, and Holloway (1965) in their general circulation model of the atmosphere. Bryan (1963) extended the kinetic energy conserving scheme to the system of the irregular grid. This method was then used by Grimmer and Shaw (1967) in their integration of the free-surface model on the sphere and by Kurihara and Holloway (1967) in the integration of a nine-level primitive model of the atmosphere with the so-called box method.

The main purpose of this study is to compare the accuracy and stability of some of the finite-difference schemes used in these integrations and to see whether

¹ A part of this work was done while the author was visiting NCAR with a NATO Research Associateship in Meteorology.

² Present address: University of Oslo, Blindern, Oslo, Norway.

other finite-difference schemes will give more accurate and stable integrations. Since all the schemes used are of second-order accuracy, the results will be compared in particular with the results of the integrations using fourth-order schemes in space. The accuracy of the integrations depends also on the resolution in the model, and the solutions will therefore be examined when the number of grid points are increased.

Long-term integrations using the leapfrog method or midpoint rule in time may lead to instability of the integration from the increase of energy on the computational modes. This instability is demonstrated, and it is shown that elimination of the computational modes by using a smoothing operator in time or by using other time-integration methods, which damp the computational modes, will improve the stability of the integration.

2. THE MODEL AND BOUNDARY CONDITION

The model used to test the different finite-difference schemes is the same model used by Houghton, Kasahara, and Washington (1966); it is a free-surface model, which describes divergent barotropic motion in an inviscid, incompressible, hydrostatic fluid with vanishing stress at its upper boundary, and the fluid is assumed confined in a channel corresponding to a middle-latitude band on the earth. The southern and northern boundaries are rigid walls where the normal velocity components vanish, and it is assumed that the flow is periodic in the west-east direction with a wavelength equal to the length of the channel. A β -plane approximation is used.

Using a Cartesian coordinate system with the x -axis in the west-east direction and the y -axis in the south-north direction, the equations for the model in Eulerian form are:

$$\frac{\partial u}{\partial t} + u \frac{\partial u}{\partial x} + v \frac{\partial u}{\partial y} - fv + \frac{\partial \phi}{\partial x} = 0, \quad (1)$$

$$\frac{\partial v}{\partial t} + u \frac{\partial v}{\partial x} + v \frac{\partial v}{\partial y} + fu + \frac{\partial \phi}{\partial y} = 0, \quad (2)$$

and

$$\frac{\partial \phi}{\partial t} + \frac{\partial(\phi u)}{\partial x} + \frac{\partial(\phi v)}{\partial y} = 0. \quad (3)$$

The velocities u and v are in the x and y direction, respectively, and $\phi = gh$ is the geopotential of the fluid, where g is the acceleration of gravity and h is the height of the free surface; f is the Coriolis parameter. These equations conserve the integrals of mass and total energy in the channel. The equation for the total energy is:

$$E = \frac{1}{2g} \int_{\sigma} (u^2 + v^2 + \phi) d\sigma \quad (4)$$

where σ is the total area of integration. The available energy in the model will be defined as:

$$AE = E - \frac{\bar{\sigma}\bar{\phi}^2}{2g} \quad (5)$$

where $\bar{\phi}$ is the average value of the geopotential of the free surface. The equations for the model may also be written in momentum form, and instead of equations (1) and (2) we may use:

$$\frac{\partial \phi u}{\partial t} + \frac{\partial}{\partial x}(\phi u u) + \frac{\partial}{\partial y}(\phi u v) - f\phi v + \phi \frac{\partial \phi}{\partial x} = 0 \quad (6)$$

and

$$\frac{\partial \phi v}{\partial t} + \frac{\partial}{\partial x}(\phi v u) + \frac{\partial}{\partial y}(\phi v v) + f\phi u + \phi \frac{\partial \phi}{\partial y} = 0. \quad (7)$$

To make the coding of the finite-difference equations easier, the following nondimensional variables are introduced:

$$\begin{aligned} x' &= \frac{x}{\Delta s}, & y' &= \frac{y}{\Delta s}, \\ t' &= \frac{t}{\Delta t}, & u' &= \frac{u \Delta t}{\Delta s}, \\ v' &= \frac{v \Delta t}{\Delta s}, & \phi' &= \phi \left(\frac{\Delta t}{\Delta s} \right)^2, \end{aligned}$$

and

$$f' = f \Delta t$$

where Δs is a grid increment in space, and Δt is a time increment. With these transformations, all the equations for the model are the same except that all the variables are the marked variables. In the following we shall, however, omit the markings.

3. FINITE-DIFFERENCE OPERATORS AND CONSERVATIVE REQUIREMENTS

In the calculations we will use a regular grid with horizontal spacing $\Delta x = \Delta y = \Delta$ and with time increment Δt ; though all the variables are not necessarily defined in each grid point, they can be staggered in time and space. To derive the finite-difference equations, we will use the following sum and difference operators adopted by Shuman (1962):

$$\alpha_x = \frac{1}{\Delta} \left[\alpha \left(x_i + \frac{\Delta}{2} \right) - \alpha \left(x_i - \frac{\Delta}{2} \right) \right], \quad (8)$$

$$\bar{\alpha}^x = \frac{1}{2} \left[\alpha \left(x_i + \frac{\Delta}{2} \right) + \alpha \left(x_i - \frac{\Delta}{2} \right) \right], \quad (9)$$

$$\bar{\alpha}^{2x} = \frac{1}{2} [\alpha(x_i + \Delta) + \alpha(x_i - \Delta)], \quad (10)$$

and

$$\begin{aligned}\overline{\alpha^{xx}} &\equiv \overline{(\alpha^x)^x} = \alpha + \frac{\Delta^2}{4} \alpha_{xx} \\ &= \frac{1}{4} [\alpha(x_i + \Delta) + \alpha(x_i - \Delta) + 2\alpha(x_i)]\end{aligned}\quad (11)$$

where α is an arbitrary function of the discrete variable $x_i = i\Delta$. Second- and fourth-order finite-difference approximations to the first and second derivatives of α can then be written:

$$\frac{\partial \alpha}{\partial x} = \overline{\alpha^x} + 0(\Delta^2), \quad (12)$$

$$\frac{\partial \alpha}{\partial x^2} = \frac{4}{3} \overline{\alpha^x} - \frac{1}{3} \overline{\alpha^{2x}} + 0(\Delta^4), \quad (13)$$

$$\frac{\partial^2 \alpha}{\partial x^2} = \alpha_{xx} + 0(\Delta^2), \quad (14)$$

and

$$\frac{\partial^2 \alpha}{\partial x^2} = \frac{4}{3} \alpha_{xx} - \frac{1}{3} \alpha_{2x2x} + 0(\Delta^4). \quad (15)$$

In order to derive conservative finite-difference schemes for the nonlinear terms in (1), (2), (3), (6), and (7), it is convenient to use the following set of identities, which may be derived from the operators (8) through (11);

$$(\alpha\beta)_x \equiv \overline{\alpha^x} \beta_x + \overline{\beta^x} \alpha_x, \quad (16)$$

$$\overline{(\alpha\beta)^x} \equiv \overline{\alpha^{2x-x}} \beta_x + \overline{\beta^{2x-x}} \alpha_x, \quad (17)$$

and

$$\begin{aligned}(\overline{\alpha\beta})^x &\equiv \overline{\alpha^{xx-x}} \beta_x + \overline{\beta^{xx-x}} \alpha_x \\ &\equiv \frac{1}{2} [(\overline{\alpha\beta})^x + \overline{\alpha\beta^x} + \overline{\beta\alpha^x}]\end{aligned}\quad (18)$$

where α and β are arbitrary functions of the discrete variable $x_i = i\Delta$.

Total energy conservative finite-difference schemes for the momentum form of the equations are the same as those derived by Lilly (1965) and used by Grimmer and Shaw (1967) and by Kurihara and Holloway (1967), and they will be given in section 5. Here we shall look more closely at the so-called conservative schemes and the quadratic conservative schemes (or schemes that conserve the first and second statistical moment of the variables). Consider the equation:

$$\frac{\partial \alpha}{\partial t} + \nabla \cdot (\mathbf{v}\alpha) = 0 \quad (19)$$

where α is an arbitrary variable, \mathbf{v} is a two- or three-

dimensional velocity vector, and ∇ is a two- or three-dimensional divergence operator. If (19) is integrated over a closed domain V , the mean value of α is conserved, and if we multiply (19) by α and again integrate over the closed domain V , the equation for the mean variance of α becomes:

$$\frac{\partial}{\partial t} \int_V \frac{\alpha^2}{2} dv = - \int_V \frac{\alpha^2}{2} \nabla \cdot \mathbf{v} dv. \quad (20)$$

The finite-difference schemes for (19), which only conserve the mean value of α , are called conservative schemes; finite-difference schemes that conserve the mean value of α , and for which the finite-difference equation for the mean variance can be written in a finite-difference form analogous to (20), will be called quadratic conservative schemes. For a regular grid in two dimensions, the simplest second-order conservative scheme for (19) is:

$$\overline{\alpha_t^x} + \overline{(\alpha u)_x} + \overline{(\alpha v)_y} = 0. \quad (21)$$

As shown in section 6, numerical integrations with this type of scheme are relatively computationally unstable if additional smoothing of the solutions is not used. The solution may be smoothed by adding a linear or nonlinear artificial viscosity term to the equation (see von Neumann and Richtmyer, 1950), or we may use time integration methods that also introduce artificial viscosity terms in the equations, as Lax and Wendroff methods (1960).

Another way to smooth the solution is to use a nine-point formula in space for the finite-difference approximation to the nonlinear terms, as done by Shuman and Vanderman (1966). The finite-difference equation for (19) may then be written:

$$\overline{\alpha_t^x} + \overline{[(\overline{\alpha^y u^y})_x + (\overline{\alpha^x v^x})_y]}^{xy} = 0 \quad (22)$$

or with the use of (9) and (11) as:

$$\begin{aligned}\overline{\alpha_t^x} + \overline{(\alpha u)_x} + \overline{(\alpha v)_y} + \frac{\Delta^2}{8} \{ [(\overline{\alpha u})_{yy} + \overline{\alpha u_{yy}} + \overline{\alpha u_{yy}}]_x \\ + [(\overline{\alpha v})_{xx} + \overline{\alpha v_{xx}} + \overline{\alpha v_{xx}}]_y \} = 0.\end{aligned}\quad (23)$$

The two last terms represent a form of nonlinear smoothing, which does not alter the conservative properties of the scheme. Another form of the nine-point scheme is used by Jelesnianski (1967) and Gates (1968) in ocean circulation calculations.

Quadratic conservative schemes for (19) have been developed by Lilly (1965) and by Bryan (1966). For a regular grid in two dimensions, these schemes may be written:

$$\overline{\alpha_t^x} + \overline{(\alpha^x u_s)_x} + \overline{(\alpha^y v_s)_y} = 0 \quad (24)$$

where u_s and v_s are the average normal velocity components at the boundary of the grid element with sides Δ which surrounds the grid point. If u and v are defined in the same grid points as α , we may define $u_s = \bar{u}^x$ and $v_s = \bar{v}^y$, and we may get a nonlinear smoothing of the solution by defining $u_s = \bar{u}^{xy}$ and $v_s = \bar{v}^{yz}$.

The quadratic conservative property of (24) is easily demonstrated by multiplying by α and adding over all the grid points j, k . The finite-difference equation for the mean variance is then:

$$\sum_{jk} \alpha \bar{\alpha}_t^i = - \sum_{jk} [\alpha (\bar{\alpha}^x u_s)_x + \alpha (\bar{\alpha}^y v_s)_y]. \quad (25)$$

Using the identities (11) and (16) gives:

$$\begin{aligned} \sum_{jk} \alpha \bar{\alpha}_t^i = & - \sum_{jk} \left[\frac{1}{2} \alpha \bar{\alpha}^{2x} u_{sx} + \alpha \bar{\alpha}^x \bar{u}_s^x + \frac{1}{2} \alpha \bar{\alpha}^{2y} v_{sy} + \alpha \bar{\alpha}^y \bar{v}_s^y \right] \\ & - \sum_{jk} \frac{1}{2} \alpha^2 (u_{sx} + v_{sy}). \end{aligned} \quad (26)$$

If the first sum on the right-hand side is written out using the operators (8) through (10), we can show that this sum is zero and therefore:

$$\sum_{jk} \alpha \bar{\alpha}_t^i = - \sum_{jk} \frac{1}{2} \alpha^2 (u_{sx} + v_{sy}) \quad (27)$$

which is a finite-difference form analogous to the analytic equation (20).

Let us instead of equation (19) consider the following advection equation:

$$\frac{\partial \alpha}{\partial t} + \mathbf{v} \cdot \nabla \alpha = 0. \quad (28)$$

We will also try to find a quadratic conservative scheme for this equation. Integrating again over a closed domain V , the equation for the mean variance of α is:

$$\int_V \frac{1}{2} \frac{\partial \alpha^2}{\partial t} dv = \int_V \frac{\alpha^2}{2} \nabla \cdot \mathbf{v} dv. \quad (29)$$

Equation (28) may be written:

$$\frac{\partial \alpha}{\partial t} + \nabla \cdot (\mathbf{v} \alpha) - \alpha \nabla \cdot \mathbf{v} = 0. \quad (30)$$

Using the finite-difference scheme (24) for $\nabla \cdot (\mathbf{v} \alpha)$ then gives the following quadratic conservative scheme for (28):

$$\bar{\alpha}_t^i + (\bar{\alpha}^x u_s)_x + (\bar{\alpha}^y v_s)_y - \alpha (u_{sx} + v_{sy}) = 0. \quad (31)$$

The finite-difference equation for the mean variance of α becomes:

$$\sum_{jk} \alpha \bar{\alpha}_t^i = \sum_{jk} \frac{1}{2} \alpha^2 (u_{sx} + v_{sy}), \quad (32)$$

which is a finite-difference equation analogous to (29). If $u_s = \bar{u}^x$ and $v_s = \bar{v}^y$, (31) becomes:

$$\bar{\alpha}_t^i + \frac{1}{2} [(\bar{\alpha} u)_x + u \bar{\alpha}_x + (\bar{\alpha} v)_y + v \bar{\alpha}_y - \alpha (\bar{u}_x + \bar{v}_y)] = 0 \quad (33)$$

or with the use of the operators (8) through (10) as:

$$\bar{\alpha}_t^i + \bar{u}^x \alpha_x + \bar{v}^y \alpha_y = 0, \quad (34)$$

which is the same scheme as Shuman's semimomentum form (1962) and the same scheme used by Matsuno (1966).

When α , u , and v are given in the same grid points, fourth-order quadratic conservative schemes in space for (19) and (28) may be written in the same form as (21), (24), and (33), where the fourth-order finite-difference (13) is used instead of the second-order difference in space.

If the flow is nondivergent, $\nabla \cdot \mathbf{v} = 0$, the source terms at the right-hand side of (27) and (32) are zero. If there are no time truncation errors, the mean variance of α will be conserved, and we may then assume that the numerical integrations of (24) and (31) are free of nonlinear computational instability as defined by Phillips (1959). But for a divergent flow, $\nabla \cdot \mathbf{v} \neq 0$, the source terms are not zero, and we cannot guarantee that the errors in the source terms may not lead to fictitious increase of mean variance that will give rise to computational instability of the integration.

4. ERRORS IN THE FINITE-DIFFERENCE EQUATIONS

The two main sources of error in approximating equations (19) and (28) by the finite-difference equations are: one, the derivatives in space and time are approximated by truncated Taylor series with second- or fourth-order accuracy; and two, instead of an infinite wave spectrum we have a limited wave spectrum, which is determined by the total number of grid points in the area of integration. Some of the errors may be reduced by making a Fourier transform of the equations and by solving the corresponding spectral equations instead of the finite-difference equations. In the following, let us look at the difference between the spectral equations for (19) and (28) and their finite-difference approximations. We shall assume that we are using the same number of waves in the spectral equations as can be resolved in the finite-difference equations.

The equations (19) and (28) are made nondimensional with the same transformations as in section 2. For α , u , and v in the grid point $x=j$, $y=k$, and $t=r$, we may then use the following Fourier substitutions:

$$\alpha(j, k, r) = \sum_{m,n} \hat{\alpha}_{m,n}^r e^{i(mj+nk)}, \quad (35)$$

$$u(j, k, r) = \sum_{m,n} \hat{u}_{m,n}^r e^{i(mj+nk)}, \quad (36)$$

and

$$v(j, k, r) = \sum_{m, n} \hat{v}_{m, n}^r e^{i(mj + nk)}. \quad (37)$$

The wave numbers m and n are in the x - and y -directions, respectively, and $\hat{\alpha}_{m, n}^r$, $\hat{u}_{m, n}^r$, and $\hat{v}_{m, n}^r$ are the time-dependent amplitudes of α , u , and v at wave number m, n . If the number of grid points in the x -direction is $2M+1$ and in the y -direction $2N+1$, the wave numbers m and n will have the values:

$$m = 0, \pm \frac{\pi}{M}, \pm \frac{2\pi}{M}, \dots, \pm \frac{(M-1)\pi}{M}, \pm \pi$$

and

$$n = 0, \pm \frac{\pi}{N}, \pm \frac{2\pi}{N}, \dots, \pm \frac{(N-1)\pi}{N}, \pm \pi$$

Introducing (35) through (37) into (19) gives the following spectral equation for $\hat{\alpha}_{m, n}^r$;

$$(\hat{\alpha}_{m, n}^r)_t + i \sum_{p, q} (m \hat{\alpha}_{p, q}^r \hat{u}_{p', q'}^r + n \hat{\alpha}_{p, q}^r \hat{v}_{p', q'}^r) = 0 \quad (38)$$

where $p + p' = m$ and $q + q' = n$.

Second- and fourth-order finite differences for the first derivative of α may be written:

$$\bar{\alpha}_x^2 = \sum_{m, n} i \sin m \hat{\alpha}_{m, n}^r e^{i(mj + nk)} \quad (39)$$

and

$$\frac{4}{3} \bar{\alpha}_x^2 - \frac{1}{3} \bar{\alpha}_{2x}^2 = \sum_{m, n} i \left(\frac{4}{3} \sin m - \frac{1}{6} \sin 2m \right) \hat{\alpha}_{m, n}^r e^{i(mj + nk)}. \quad (40)$$

Introducing these into the finite-difference equations (21) and (24) with $u_s = \bar{u}^x$ and $v_s = \bar{v}^y$ gives:

$$(\hat{\alpha}_{m, n}^r)_t + i \sum_{p, q} (s^m \hat{\alpha}_{p, q}^r \hat{u}_{p', q'}^r + s^n \hat{\alpha}_{p, q}^r \hat{v}_{p', q'}^r) = 0 \quad (41)$$

and

$$(\hat{\alpha}_{m, n}^r)_t + i \sum_{p, q} (s_p^m \hat{\alpha}_{p, q}^r \hat{u}_{p', q'}^r + s_q^n \hat{\alpha}_{p, q}^r \hat{v}_{p', q'}^r) = 0 \quad (42)$$

where

$$p + p' = \begin{cases} m \\ m - \frac{2\pi m}{|m|} \end{cases} \text{ and } q + q' = \begin{cases} n \\ n - \frac{2\pi n}{|n|} \end{cases}$$

For the second-order finite-difference schemes:

$$s^m \equiv s(\Delta^2)^m = \sin m$$

and

$$s_p^m \equiv s(\Delta^2)_p^m = \frac{1}{2} (\sin m + \sin p + \sin p'),$$

and for fourth-order finite differences:

$$s^m \equiv s(\Delta^4)^m = \frac{4}{3} \sin m - \frac{1}{6} \sin 2m$$

and

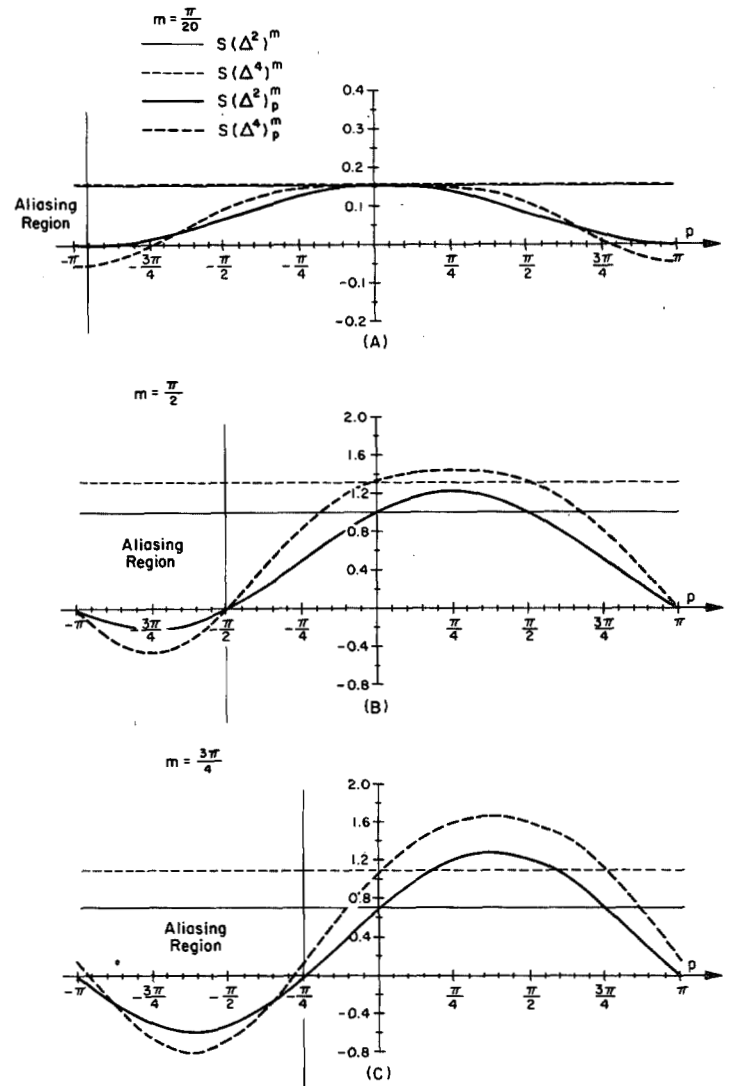


FIGURE 1.—The interaction coefficients $s^m s_p^m$ as a function of the wave number p for $m = \pi/20$, $\pi/2$, and $3\pi/4$.

$$s_p^m \equiv s(\Delta^4)_p^m = \frac{4}{6} [\sin m + \sin p + \sin p']$$

$$- \frac{1}{12} [\sin 2m + \sin 2p + \sin 2p'].$$

The three sums, when $p + p' = m$ and $q + q' = n - \frac{2\pi n}{|n|}$, when $p + p' = m - \frac{2\pi m}{|m|}$ and $q + q' = n$; and when $p + p' = m - \frac{2\pi m}{|m|}$ and $q + q' = n - \frac{2\pi n}{|n|}$, represent the aliasing errors in the finite-difference equations. The truncation errors (or the derivative errors) introduced by the finite-difference approximations to the derivatives are the differences between m and s^m or s_p^m and between n and s^n or s_q^n . The interaction coefficients s^m and s_p^m for $m = \pi/20$, $\pi/2$, and $3\pi/4$ are given in figure 1. This shows that for $0 \leq p \leq m$, $s_p^m \geq s^m$, and the quadratic conservative scheme has in that part of the spectrum smaller truncation

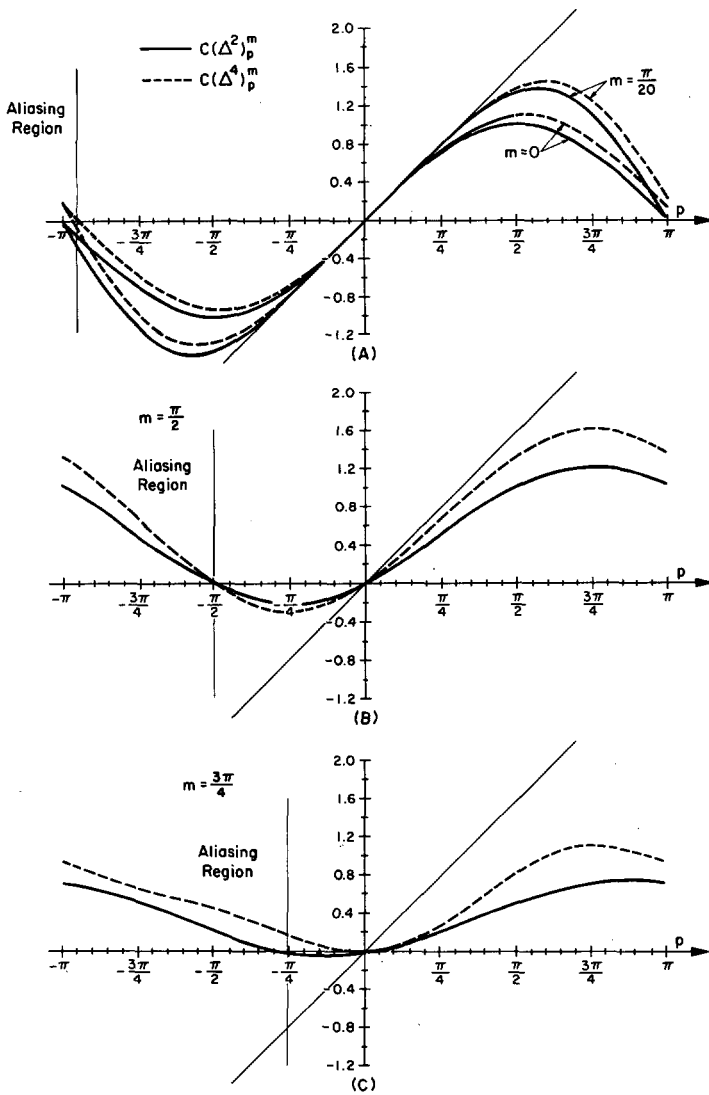


FIGURE 2.—The interaction coefficients c^m and c_p^m as a function of the wave number p for $m=0$, $\pi/20$, $\pi/2$, and $3\pi/4$.

errors than the conservative scheme; but for $p > m$ and $p < 0$, the truncation errors in the quadratic conservative scheme increase. At the same time s_p^m becomes smaller in magnitude, and the contribution to the sum in (42) from these parts of the spectrum, which contains the small scale, becomes smaller. For the aliasing terms, we see that $|s_p^m| < |s^m|$, and the quadratic conservative scheme, therefore, has smaller aliasing errors than the conservative scheme. When fourth-order schemes are used, we see that the truncation errors decrease, but at the same time the magnitude of the interaction coefficients for the aliasing terms increase.

The Fourier transform of the advective equation (28) and the finite-difference equation (33) may be written:

$$\overline{(\hat{\alpha}_{m,n})}^t + \sum_{p,q} (p \hat{\alpha}_{p,q}^r \hat{u}_{p',q'}^r + q \hat{\alpha}_{p,q}^r \hat{v}_{p',q'}^r) = 0 \quad (43)$$

where

$$p + p' = m \text{ and } q + q' = n,$$

and

$$\overline{(\hat{\alpha}_{m,n})}^t + \sum_{p,q} (c_p^m \hat{\alpha}_{p,q}^r \hat{u}_{p',q'}^r + c_q^n \hat{\alpha}_{p,q}^r \hat{v}_{p',q'}^r) = 0 \quad (44)$$

where

$$p + p' = \begin{cases} m \\ m - \frac{2\pi m}{|m|} \end{cases} \text{ and } q + q' = \begin{cases} n \\ n - \frac{2\pi n}{|n|} \end{cases}$$

$$c(\Delta^2)_p^m = \frac{1}{2} (\sin m + \sin p - \sin p'),$$

and

$$c(\Delta^4)_p^m = \frac{4}{6} (\sin m + \sin p - \sin p')$$

$$- \frac{1}{12} (\sin 2m + \sin 2p - \sin 2p')$$

for second- and fourth-order finite-difference schemes, respectively. The truncation errors in (44) are the differences between p and the interaction coefficient c_p^m and between q and c_q^n , and the aliasing errors are again the contributions to the sum when $p + p' = m$ and $q + q' = n - \frac{2\pi n}{|n|}$; when $p + p' = m - \frac{2\pi m}{|m|}$ and $q + q' = n$; and when $p + p' = m - \frac{2\pi m}{|m|}$ and $q + q' = n - \frac{2\pi n}{|n|}$.

The interaction coefficients c_p^m for $m=0$, $\pi/20$, $\pi/2$, and $3\pi/4$ are given in figure 2. We see again that the truncation errors increase with increasing m , and that the fourth-order scheme has smaller truncation errors; but especially for large m the aliasing errors are larger than for the second scheme.

If we want to smooth the solution of the advection equation (28) by applying a nine-point formula in space for the derivatives, the finite-difference equations for (28) may be written:

$$\bar{\alpha}_t^t + \bar{n}^x \alpha_x^{xy} + \bar{v}^y \alpha_y^{yz} = 0 \quad (45)$$

or

$$\bar{\alpha}_t^t + \bar{u}^x \alpha_x^{xy} + \bar{v}^y \alpha_y^{yz} = 0. \quad (46)$$

The Fourier transforms of these finite-difference equations are:

$$(\hat{\alpha}_{m,n}^r)_t + i \sum_{p,q} (d_{p,q}^{m,n} \hat{\alpha}_{p,q}^r \hat{u}_{p',q'}^r + d_{p,q}^{n,m} \hat{\alpha}_{p,q}^r \hat{v}_{p',q'}^r) = 0 \quad (47) \quad \text{BOUNDARY}$$

and

$$(\hat{\alpha}_{m,n}^r)_t + i \sum_{p,q} (d_{p,q}^{m,n} \hat{\alpha}_{p,q}^r \hat{u}_{p',q'}^r + d_{p,q}^{n,m} \hat{\alpha}_{p,q}^r \hat{v}_{p',q'}^r) = 0 \quad (48)$$

where

$$p+p' = \begin{cases} m \\ m - \frac{2\pi m}{|m|} \end{cases} \text{ and } q+q' = \begin{cases} n \\ n - \frac{2\pi n}{|n|} \end{cases}$$

$$|d_{p,q}^{m,n}| = |c_p^m \frac{1+\cos n}{2}| \leq |c_p^m|$$

and

$$|d_{p,q}^{m,n}| = |c_p^m \cos \frac{n}{2} \cos \frac{q}{2} \cos \frac{q'}{2}| \leq |c_p^m|$$

The truncation errors in (45) and (46) will therefore be at least as large as in (33), but the aliasing errors will be smaller. As either m or n goes to $\pm\pi$, the interaction coefficients $d_{p,q}^{m,n}$ and $d_{p,q}^{n,m}$ go to zero. This means that waves with wave numbers $m = \pm\pi$ or $n = \pm\pi$ (waves with wavelength equal to two grid increments) cannot be formed in the second-order finite-difference equations (45) and (46).

If (45) and (46) are linearized by assuming $u=U=\text{constant}$ and $v=0$, the equations (47) and (48) reduce to:

$$(\hat{\alpha}_{m,n}^r)_t + iU \sin m \left(\frac{1+\cos n}{2} \right) \hat{\alpha}_{m,n}^r = 0. \quad (49)$$

The amplification matrix for (49) may be written:

$$\omega^2 + 2iU \sin m \left(\frac{1+\cos n}{2} \right) \omega - 1 = 0 \quad (50)$$

where ω is the eigenvalue. The roots of (50) are:

$$\omega_{1,2} = -iU \sin m \left(\frac{1+\cos n}{2} \right) \pm \sqrt{-\left[U \sin m \left(\frac{1+\cos n}{2} \right) \right]^2 + 1}$$

with the magnitudes:

$$|\omega_{1,2}| = 1, \text{ for } |U| \leq 1.$$

For the linearized equation this form of smoothing will not change the amplitude of the solution or the linear stability condition, but the error in the phase speed of the wave

$$\epsilon = U - \frac{\arcsin \left[U \sin m \left(\frac{1+\cos n}{2} \right) \right]}{m} \quad (51)$$

will increase with increasing n . Therefore, in the finite-

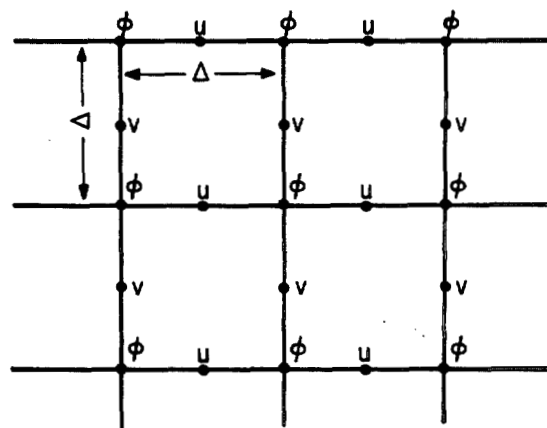


FIGURE 3.—The location of u , v , and ϕ in the grid when using Lilly's Scheme C and the generalized Arakawa Scheme I.

difference equations (45) and (46), we may expect larger phase errors than in the finite-difference equation (33).

5. FINITE-DIFFERENCE SCHEMES FOR THE EQUATIONS FOR THE MODEL

By applying the finite-difference formulations given in section 3, finite-difference schemes which are either spatial conservative, quadratic conservative, or total energy conservative, or finite-difference schemes where the derivatives are calculated over nine grid points in space may be derived for the equations for the model. To find the differences in the stability, the energy distribution, and the phase speed of the waves for the different types of schemes, the following sets of finite-difference equations are used for the momentum equations (6), (7), and (3):

Scheme A—the quadratic conservative momentum scheme whereby

$$\begin{aligned} (\overline{\phi u})_t + (\overline{\phi u}^x)_x + (\overline{\phi u}^y)_y - f\phi v + \frac{1}{2}(\overline{\phi^2})_x &= 0, \\ (\overline{\phi v})_t + (\overline{\phi v}^x)_x + (\overline{\phi v}^y)_y + f\phi u + \frac{1}{2}(\overline{\phi^2})_y &= 0, \end{aligned} \quad (52)$$

and

$$\overline{\phi}_t + (\overline{\phi}^x)_x + (\overline{\phi}^y)_y = 0.$$

Each of the equations is written as a spatial quadratic conservative finite-difference equation in the nonlinear terms. This scheme will not conserve the total energy; but for $\phi = \text{constant}$, the kinetic energy will be conserved.

Scheme B—the total energy conservative momentum scheme is the same as used by Grimmer and Shaw (1967) for a free-surface model on the sphere. For a plane model the finite-difference equations are:

$$\begin{aligned} (\overline{\phi u})_t + (\overline{\phi u}^x)_x + (\overline{\phi u}^y)_y - f\phi v + \phi \phi_x &= 0, \\ (\overline{\phi v})_t + (\overline{\phi v}^x)_x + (\overline{\phi v}^y)_y + f\phi u + \phi \phi_y &= 0, \end{aligned} \quad (53)$$

and

$$\overline{\phi}_t + (\overline{\phi}^x)_x + (\overline{\phi}^y)_y = 0.$$

The total energy equation may be written:

$$\sum_{jk} \left[u(\overline{\phi u})_i + v(\overline{\phi v})_i - \frac{u^2 + v^2}{2} \overline{\phi}_i + \phi \overline{\phi}_i \right] = 0, \quad (54)$$

or

$$\frac{1}{2} \sum_{jk} \left[(u^2 + v^2 + \phi) \overline{\phi} \right]_i = - \frac{(\Delta t)^2}{2} \sum_{jk} \left\{ u_{ii} (\overline{\phi u})_i + v_{ii} (\overline{\phi v})_i + \left(\frac{u^2 + v^2}{2} \right)_{ii} \overline{\phi}_i + \phi_{ii} \overline{\phi}_i - \frac{\Delta^2}{2} \left[(u_{ii})^2 + (v_{ii})^2 \right] \overline{\phi}_i \right\}. \quad (55)$$

The conservation of total energy will, therefore, depend on the second derivative in time of the variables when the leapfrog method is used.

Scheme C—Lilly's scheme whereby

$$\begin{aligned} \overline{(\phi^x u)}_i + \overline{(\phi^x u^x)}_x + \overline{(\phi^y v^x)}_y - f \overline{\phi^x v} + \overline{\phi^x} \phi_x &= 0, \\ \overline{(\phi^y v)}_i + \overline{(\phi^y v^x)}_x + \overline{(\phi^y v^y)}_y + f \overline{\phi^y u} + \overline{\phi^y} \phi_y &= 0, \end{aligned} \quad (56)$$

and

$$\overline{\phi}_i + (\overline{\phi^x u})_x + (\overline{\phi^y v})_y = 0.$$

This finite-difference scheme is derived by Lilly (1965) and differs from Scheme B in that the velocity components u and v are not defined in the same grid points as ϕ but are staggered in space as given in figure 3.

By linearizing these equations and neglecting the coriolis terms, we find the linear stability condition for this scheme to be, approximately:

$$C \frac{\Delta t}{\Delta} \lesssim \frac{1}{2}, \text{ when } |U| \ll C,$$

compared to:

$$(|U| + C) \frac{\Delta t}{\Delta} \leq 1$$

for Schemes A and B. U is the mean zonal velocity, and $C = \sqrt{gH}$, where H is the mean height of the free surface. The difference in the linear stability conditions follows from the fact that some of the derivatives in the Scheme C are approximated by finite differences over one grid increment only, compared to two grid increments in Schemes A and B. If the same grid increment in space is used in the schemes, the time increment in Scheme C has to be approximately half of the time increment used in Schemes A and B.

Scheme D—the time-staggered momentum scheme whereby

$$\begin{aligned} \overline{(\phi u)}_i + \overline{(\phi u u)}_x + \overline{(\phi u v)}_y - f \overline{\phi v} + \frac{1}{2} \overline{(\phi^2)}_x &= 0, \\ \overline{(\phi v)}_i + \overline{(\phi v u)}_x + \overline{(\phi v v)}_y + f \overline{\phi u} + \frac{1}{2} \overline{(\phi^2)}_y &= 0, \end{aligned} \quad (57)$$

and

$$\overline{\phi}_i + \overline{(\phi u)}_x + \overline{(\phi v)}_y = 0.$$

This scheme is used because it is economical in storage and is fast, since only half as many grid points are needed as in the other schemes. But the scheme has no quadratic conservative properties, and the integrations become computationally unstable after a short time without additional smoothing of the solutions.

For the equations in advective form (1), (2), and (3), the following sets of finite-difference equations will be used:

Scheme E—the equations (1) and (2) may also be written as:

$$\frac{\partial u}{\partial t} + \frac{\partial}{\partial x} \left(\frac{u^2 + v^2}{2} + \phi \right) - v \left(f + \frac{\partial v}{\partial x} - \frac{\partial u}{\partial y} \right) = 0, \quad (58)$$

and

$$\frac{\partial v}{\partial t} + \frac{\partial}{\partial y} \left(\frac{u^2 + v^2}{2} + \phi \right) + u \left(f + \frac{\partial v}{\partial x} - \frac{\partial u}{\partial y} \right) = 0. \quad (59)$$

Using the second-order finite-difference formula (12) for all the derivatives gives the following total energy conservative advective scheme:

$$\begin{aligned} \overline{u}_i + \left(\frac{u^2 + v^2}{2} + \phi \right)_x - v(f + \overline{v}_x - \overline{u}_y) &= 0, \\ \overline{v}_i + \left(\frac{u^2 + v^2}{2} + \phi \right)_y + u(f + \overline{v}_x - \overline{u}_y) &= 0, \end{aligned} \quad (60)$$

and

$$\overline{\phi}_i + \overline{(\phi u)}_x + \overline{(\phi v)}_y = 0.$$

The equation for the total energy becomes:

$$\sum_{jk} \left\{ \phi u \overline{u}_i + \phi v \overline{v}_i + \left(\frac{u^2 + v^2}{2} + \phi \right) \overline{\phi}_i \right\} = 0, \quad (61)$$

or

$$\begin{aligned} \frac{1}{2} \sum_{jk} \left[(u^2 + v^2 + \phi) \overline{\phi} \right]_i &= + \frac{(\Delta t)^2}{2} \sum_{jk} \left\{ \phi u_{ii} \overline{u}_i + \phi v_{ii} \overline{v}_i \right. \\ &\quad \left. + \phi_{ii} \overline{\phi}_i + \phi_{ii} \left(\frac{u^2 + v^2}{2} \right)_i + \left(\frac{u^2 + v^2}{2} \right)_{ii} \overline{\phi}_i \right\}. \end{aligned} \quad (62)$$

The conservation of total energy in this scheme will therefore also depend on the second derivative in time of the variables, as in Schemes B and C.

This scheme does not conserve total momentum in the nonlinear terms, and it probably has large truncation errors since:

$$\frac{1}{2} \overline{u_y^2} - u \overline{u_y} = \frac{\Delta^2}{2} u_{yy} \overline{u_y},$$

and

$$\frac{1}{2} \overline{v_x^2} - v \overline{v_x} = \frac{\Delta^2}{2} v_{xx} \overline{v_x},$$

which are zero only when: $u_{yy} = v_{xx} = 0$ or $\overline{u_y} = \overline{v_x} = 0$.

Scheme F—the quadratic conservative advective scheme and whereby

$$\begin{aligned}\bar{u}_t^i + (\bar{u}^x \bar{u}^x)_x + (\bar{u}^y \bar{v}^y)_y - u(\bar{u}_x^x + \bar{v}_y^y) - f\bar{v} + \bar{\phi}_x^x &= 0, \\ \bar{v}_t^i + (\bar{v}^x \bar{u}^x)_x + (\bar{v}^y \bar{v}^y)_y - v(\bar{u}_x^x + \bar{v}_y^y) + f\bar{u} + \bar{\phi}_y^y &= 0,\end{aligned}\quad (63)$$

and

$$\bar{\phi}_t^i + (\bar{\phi}^x \bar{u}^x)_x + (\bar{\phi}^y \bar{v}^y)_y = 0.$$

The finite-difference equations are written in spatial quadratic conservative forms according to equations (24) and (33). The scheme will conserve total momentum in the nonlinear terms, but it will not conserve total energy. For $\phi = \text{constant}$, this scheme is identical to Scheme A.

If we want to apply a nonlinear smoother to the equations by calculating the derivatives and the Coriolis terms over nine grid points in space, the finite-difference equations may be written in the same form as the equations (45) or (46), where the finite-difference equations are basically given in a quadratic conservative form. For (1), (2), and (3), we may then use:

Scheme G—the average quadratic conservative advective scheme whereby

$$\begin{aligned}\bar{u}_t^i + \frac{1}{2} \bar{u}_x^{xy} + \bar{v}_y^{yx} - \bar{f} \bar{v}^{xy} + \bar{\phi}_x^{xy} &= 0, \\ \bar{v}_t^i + \bar{u}_x^{xy} + \frac{1}{2} \bar{v}_y^{yx} + \bar{f} \bar{u}^{xy} + \bar{\phi}_y^{xy} &= 0,\end{aligned}\quad (64)$$

and

$$\bar{\phi}_t^i + (\bar{u} \bar{\phi})_x + (\bar{v} \bar{\phi})_y = 0.$$

Scheme H—Shuman's scheme such that

$$\begin{aligned}\bar{u}_t^i + (\bar{u} \bar{u}_x + \bar{v} \bar{u}_y + \bar{\phi}_x - \bar{f} \bar{v})^{xy} &= 0, \\ \bar{v}_t^i + (\bar{u} \bar{v}_x + \bar{v} \bar{v}_y + \bar{\phi}_y + \bar{f} \bar{u})^{xy} &= 0,\end{aligned}\quad (65)$$

and

$$\bar{\phi}_t^i + [(\bar{u} \bar{\phi})_x + (\bar{v} \bar{\phi})_y]^{xy} = 0.$$

This scheme is used by Shuman and Vanderman (1966).

Scheme I—generalized Arakawa scheme whereby

$$\begin{aligned}\bar{u}_t^i + 1/3 \{ (\bar{u}^x \bar{u}^x)_x + 1/2 [\bar{u}(\bar{u} + \Delta^2 \nabla^2 \bar{u})]_x \\ + 2\bar{v} \bar{u}_y^{xy} + \bar{v}_y^{yx} - \bar{f} \bar{v}^{xy} + \bar{\phi}_x^x \} &= 0,\end{aligned}\quad (66a)$$

$$\begin{aligned}\bar{v}_t^i + 1/3 \{ 2\bar{u} \bar{v}_x^{xy} + \bar{u}_x^{xy} + (\bar{v}^y \bar{v}^y)_y \\ + 1/2 (\bar{v}(\bar{v} + \Delta^2 \nabla^2 \bar{v}))_y \} + \bar{f} \bar{u}^{xy} + \bar{\phi}_y^y &= 0,\end{aligned}\quad (66b)$$

$$\bar{\phi}_t^i + (\bar{\phi}^x \bar{u})_x + (\bar{\phi}^y \bar{v})_y = 0 \quad (66c)$$

where $\nabla^2 u = u_{xx} + u_{yy}$. The finite-difference equations in this scheme are derived in Appendix 1. For the non-divergent flow, the scheme will conserve kinetic energy, mean vorticity, and mean square vorticity. As in Lilly's scheme, u , v , and ϕ are defined in different locations in the grid. The linear stability condition for this scheme is, therefore, approximately

$$C \frac{\Delta t}{\Delta} \lesssim \frac{1}{2}, \text{ when } |U| \ll C.$$

The linear stability condition can be changed by changing u 's and v 's positions in the grid in figure 3. The last two terms in (66a) and (66b) may then be written

$$-\bar{f} \bar{v} + \bar{\phi}_x^{xy} \text{ and } \bar{f} \bar{u} + \bar{\phi}_y^{xy},$$

and instead of (66c) we get

$$\bar{\phi}_t^i + (\bar{\phi}^x \bar{u})_x + (\bar{\phi}^y \bar{v})_y = 0;$$

and the linear stability condition becomes

$$(|U| + C) \frac{\Delta t}{\Delta} \leq 1.$$

From (66a) and (66b), we see also that this scheme has nonlinear smoothing terms.

Scheme J—fourth-order quadratic conservative advective scheme has the same form as Scheme F, but all the second-order finite-difference approximations to the derivatives are exchanged with the fourth-order difference approximation (13).

6. INITIAL CONDITION

In these experiments the height of the free surface is given initially, and the velocity components u and v are calculated from the geostrophic approximation. This will introduce unwanted gravity-inertia waves in the solution, but the calculations show that their amplitudes are small. Experiments in which the velocity components were determined from the nonlinear balance equation, namely:

$$\frac{\partial^2 \phi}{\partial t^2} = \nabla \cdot [\nabla \cdot (\phi \nabla \nabla) + f \mathbf{k} \times \phi \nabla + \phi \nabla \phi] = 0 \quad (67)$$

where

$$\frac{\partial \phi}{\partial t} = \nabla \cdot (\phi \nabla) = 0 \quad (68)$$

did not improve the stability of the integrations. In our case, this probably came from the increase in the small-

TABLE 1.—Occurrence of computational instability

Scheme	Initial Condition I (days)	Initial Condition II (days)	Initial Condition III (days)
A	49	-----	16
B	49	-----	18
C	40	-----	18
D	2	-----	-----
E	31	21	11
F	49	32	16
G	98	54	28
H	-----	-----	28
I	>100	-----	64

scale kinetic energy in the adjusted velocity field; as shown in table 1, the stability of the integrations depends on the initial energy distribution. The balance equation (67) was solved by the same iterative method used by Eliassen, Grammelvedt, and Bremnes (1964).

To test the stability of the different finite-difference schemes, the initial conditions should have been given arbitrarily to get a statistical measure of which scheme gives the most stable integration. That, however, is almost impossible from a computational point of view. We have, therefore, chosen to use three different initial conditions, all describing a westerly jet flow with north-south perturbations of different wavelengths and amplitudes along the zonal axis of the jet. The initial height fields are:

$$\text{I. } h(x, y) = H_0 + H_1 \tanh \frac{9(y-y_0)}{2D} + H_2 \operatorname{sech}^2 \frac{9(y-y_0)}{D} \sin \left(\frac{2\pi x}{L} \right), \quad (69)$$

$$\text{II. } h(x, y) = H_0 + H_1 \tanh \frac{9(y-y_0)}{2D} + H_2 \operatorname{sech}^2 \frac{9(y-y_0)}{D} \left[.7 \sin \left(\frac{2\pi x}{L} \right) + .6 \sin \left(\frac{6\pi x}{L} \right) \right], \quad (70)$$

and

$$\text{III. } h(x, y) = H_0 + H_1 \tanh \frac{9(y-y_0)}{2D} + H_2 \operatorname{sech}^2 \frac{9(y-y_0)}{D} \left[.8 \sin \left(\frac{2\pi x}{L} \right) + .5 \sin \left(\frac{12\pi x}{L} \right) \right] \quad (71)$$

where L is the length, D is the width, and $y_0 = D/2$ is the middle latitude of the channel. Since the initial velocity fields are geostrophic, the height of the free surface has to be constant along the northern and southern boundaries to fulfill initially the boundary condition $v=0$. To avoid strong variation in space of the velocity field near the boundaries, H_2 is set equal to zero at the boundaries and at the two rows of grid points next to the boundaries.

In the numerical calculations the following values are adopted:

$$\begin{aligned} H_0 &= 2000 \text{ m}, & L &= 6000 \text{ km}, \\ H_1 &= -220 \text{ m}, & D &= 4400 \text{ km}, \\ H_2 &= 133 \text{ m}, & f &= 10^{-4} \text{ sec}^{-1}, \\ g &= 10 \text{ m sec}^{-2}, & \text{and } \beta &= 1.5 \cdot 10^{-11} \text{ sec}^{-1} \text{ m}^{-1}. \end{aligned}$$

The height fields for the Initial Conditions I and II are given in figure 6.

The boundary conditions used in the numerical integrations with Schemes A, B, D, E, and F are:

$$v=0, \quad \bar{\phi}_y^v=0, \quad \bar{u}_y^v=0,$$

$$\bar{v}_y^v = -2v_{n-1}, \quad \text{and} \quad \bar{v}_y^v = 2v_{s+1}$$

where v_{n-1} and v_{s+1} are the values of v in the grid points next to the northern and southern boundaries, respectively.

In the Schemes C and I, ϕ and u are given at the boundaries and v in the grid points next to the boundaries as in figure 3. The boundary conditions used are $v=0$ in the grid points next to the boundaries.

In the average Schemes G and H and in the fourth-order Scheme J, two sets of boundary conditions are needed. The simplest conditions to use are that $v=0$ at the boundary and at the grid points next to the boundary, and that u and ϕ are symmetric across the boundaries.

7. RESULTS

All the schemes are integrated with Initial Conditions I and III until instability occurs, using the leapfrog method in time with a 10-min time step, except for Scheme C and I where 5-min time steps are used, and with a basic grid of 31×23 grid points in the west-east and the south-north directions, respectively. The Schemes E, F, and G are also integrated until the integrations become unstable, using Initial Condition II. The integration is defined to be unstable when the total available energy has increased more than 10 percent above its initial value. The available energy is calculated from

$$AE = \frac{1}{2g} \sum_{jk} \{ \phi_{jk} (u_{jk}^2 + v_{jk}^2) + (\phi_{jk} - gH_0)^2 \} \quad (72)$$

where the summation is over all grid points j, k in the area of integration. The results are given in table 1. We see that the stability of the integrations depends on the initial conditions. Integrations using Initial Condition III, which initially has energy in wave numbers one and six in the x -direction, are for all the schemes much more unstable than those using Initial Condition I, which initially only has energy in wave number one in the x -direction. Using for the Schemes E, F, and G the Initial Condition II, which contains energy in wave numbers one

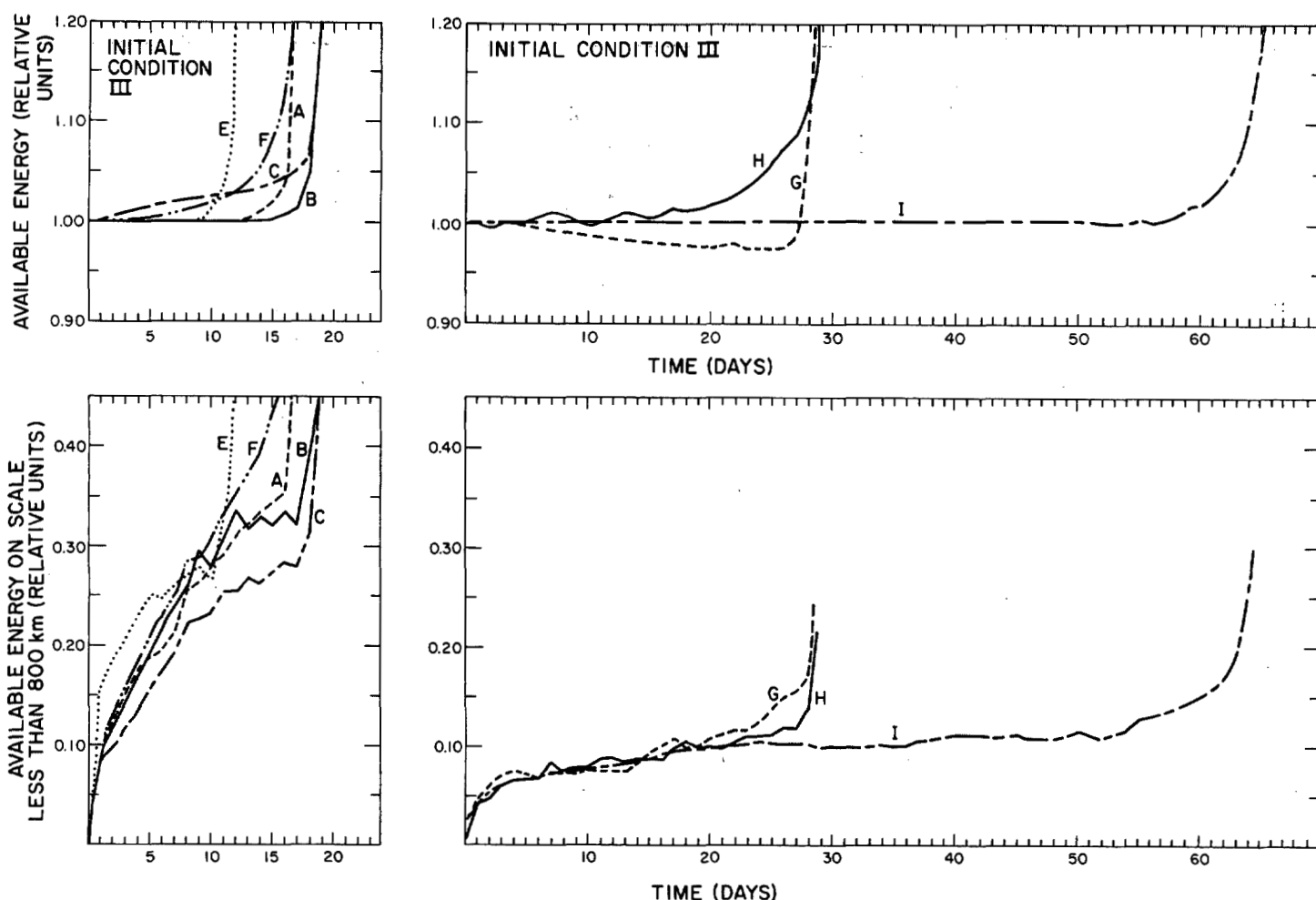


FIGURE 4.—Available energy (top) and the available energy on the scale less than 800 km (bottom) as a function of time for the different schemes using Initial Condition III and $\Delta = L/30 = 200$ km.

and three in the x -direction, the integrations became unstable after twice as long a time as when the Initial Condition III is used. We also see that the differences are small between the total energy conservative Schemes B and C and the quadratic conservative Schemes A and F. The total energy conservative advective Scheme E is more unstable, and the conservative Scheme D is, as expected, already unstable after 2 days using Initial Condition I, but the mean differences exist between the Schemes A, B, C, and F and the space average Schemes G and H and the generalized Arakawa Scheme I. For all the initial conditions, integrations with these three schemes are much more stable than integrations with the other schemes.

If we look at the variation of the available energy in time, we find that the available energy is almost constant until a short time before the instability occurs. We also notice that the available energy on the small scale, which in this study will be defined as the energy on the scale with wavelength less than 800 km, increases in time, and that the large-scale energy decreases. The small-scale energy is found by a Fourier analysis of the u , v , and ϕ fields after each day of integrations. The energy at the

wave number m , n is approximated by:

$$E_{m,n} = \frac{LD}{2} \left[H_0 (\hat{u}_{m,n}^2 + \hat{v}_{m,n}^2) + \frac{1}{g} \hat{\phi}_{m,n}^2 \right], \quad (73)$$

and the energy on the small scale is defined as:

$$ES = \sum_{m=\frac{\pi}{8M}}^{\pi} \sum_{n=\frac{\pi}{8N}}^{\pi} E_{m,n} \quad (74)$$

where the same Fourier substitutions as in section 4 are used.

The variation of available energy and small-scale energy using Initial Condition III is given in figure 4. The differences between the Schemes A, B, C, and F are again small. For all these schemes the small-scale energy increases rapidly, and after 10 days approximately 30 percent of the available energy is in the small scale. For the Schemes G, H, and I the small-scale energy increases much more slowly and is small until instability occurs. To see if the increase in the small-scale energy in the Schemes A, B, C, and F is due only to the truncation

errors and the aliasing errors in the schemes, we may decrease the timestep or we may increase the number of grid points to see if the small-scale energy increases at the same rate. For this study, Initial Condition II will be used, and since the differences between the Schemes A, B, C, and F are small, Scheme F, which has the shortest computation time for 1 day of integration, will represent the total energy conservative and the quadratic conservative schemes.

Scheme F is integrated with a grid increment $\Delta=L/30$, $\Delta=L/45$, and $\Delta=L/60$. For the two shortest grid increments the integrations are stopped after 25 days. The results are given in figure 5. This shows that when the grid increment decreases, the small-scale energy also decreases, but after several days of integration the small-scale energy again increases rapidly when the truncation errors and aliasing errors accumulate. We see also that only for the high resolution in Scheme F is the small-scale energy in the first 14 days less than the small-scale energy in Scheme G using the low resolution $\Delta=L/30$. Using a 5-min instead of a 10-min timestep in Scheme F with $\Delta=L/30$ gives little difference in the increase of the small-scale energy and in the stability. The increase of the small-scale energy is, therefore, not directly related to the truncation errors in time but is mostly due to the truncation errors and aliasing errors in space. When the low resolution is used in the fourth-order Scheme J, the increase in the small-scale energy is a little less than for Scheme F, but when the high resolution is used the difference is insignificant.

To find the errors in the amplitudes and the phase speeds of the waves, let us look at the differences between the height fields of the free surface after 5 and 10 days of integration for different schemes and resolutions. Scheme

F represents again the second-order quadratic conservative and total energy conservative schemes, since these schemes also show great similarities in the amplitudes and the phase speeds of the waves for all initial conditions.

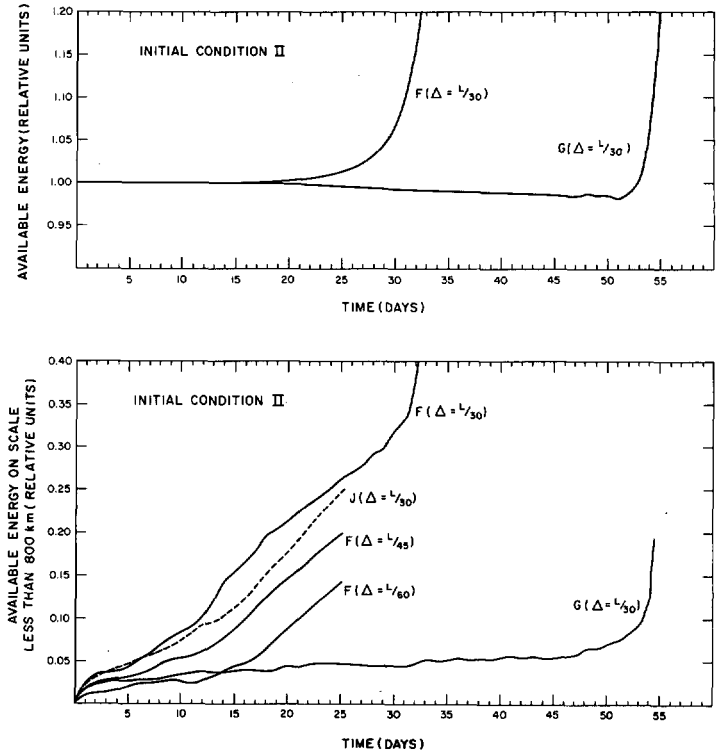


FIGURE 5.—Available energy (top) as a function of time for the Schemes F and G using Initial Condition II and $\Delta=L/30=200$ km, and available energy on the scale less than 800 km (bottom) as a function of time for Schemes F, G, and J using Initial Condition II and different grid increments.

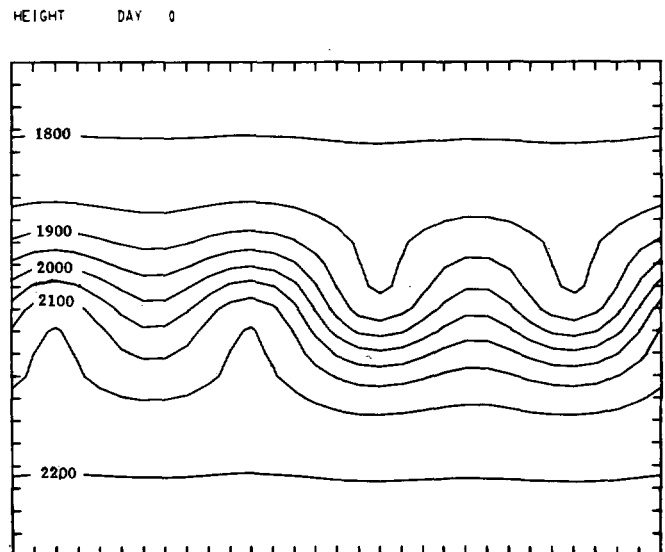
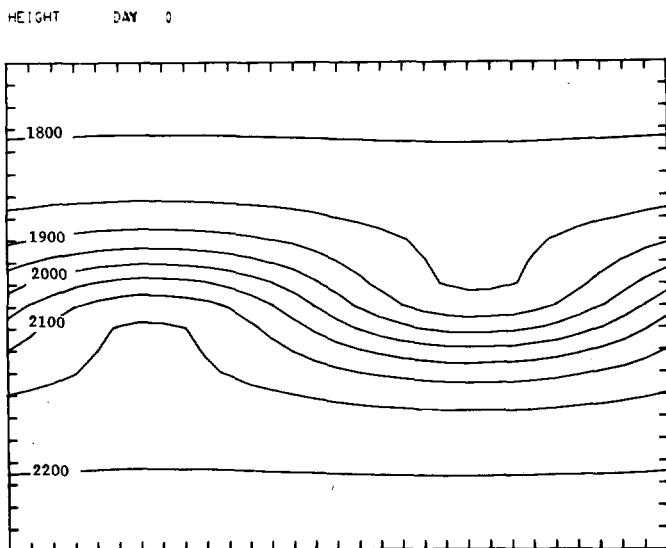


FIGURE 6.—Initial height fields (meters) for Initial Conditions I and II as used in the calculations. Contours are drawn for every 50 m.

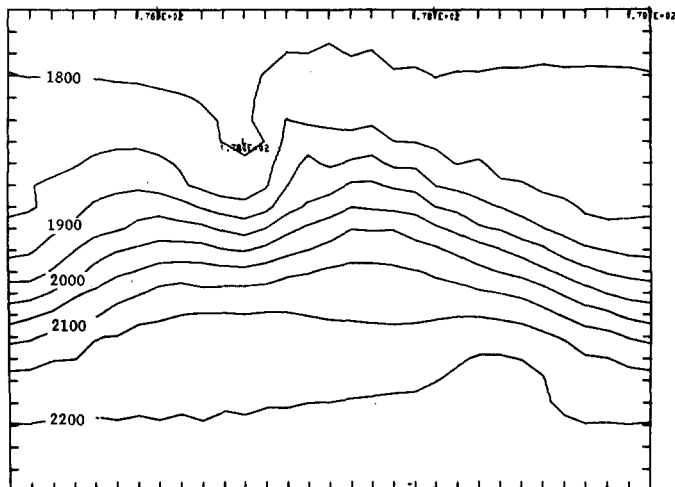
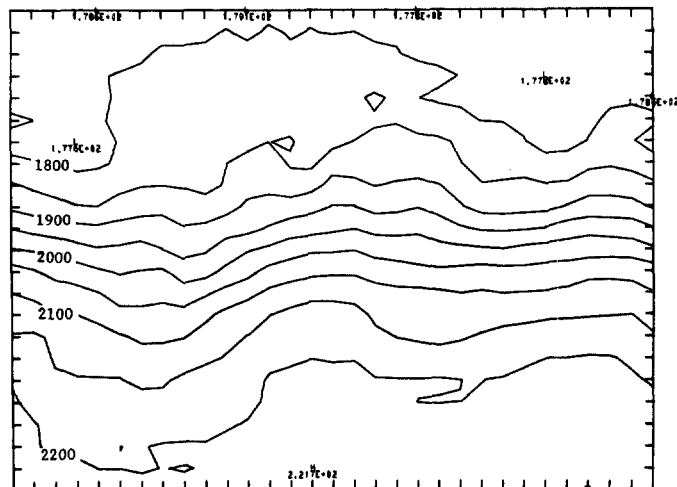
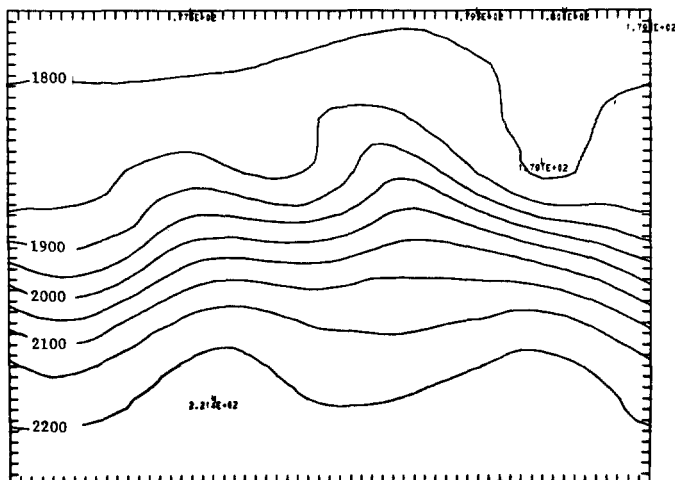
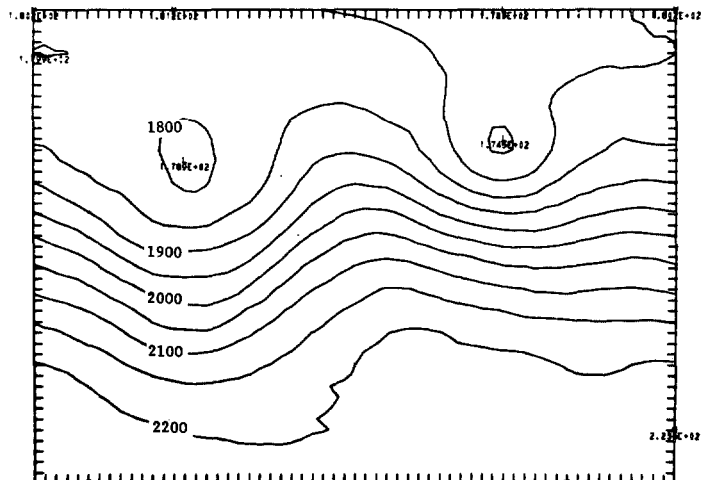
HEIGHT DAY 5, $\Delta = 200$ KMHEIGHT DAY 10, $\Delta = 200$ KMHEIGHT DAY 5, $\Delta = 100$ KMHEIGHT DAY 10, $\Delta = 100$ KM

FIGURE 7.—Height fields after 5 and 10 days of integration using the quadratic conservative advective Scheme F, Initial Condition I, and the two grid increments $\Delta = L/30 = 200$ km (top) and $\Delta = L/60 = 100$ km (bottom). The locations of the grid points are marked along the edges, and the contours are drawn for every 50 m.

The height fields for the Initial Conditions I and II are given in figure 6, and the results after 5 and 10 days using Initial Condition I and Scheme F and the two different grid increments $\Delta = L/30$ and $\Delta = L/60$ are given in figure 7. After 5 days the height fields contain mainly wave numbers one and two in the x -direction besides the zonal flow; the difference in the amplitudes of the waves between the two resolutions is small, but the weak trough to the east in the integration with the high resolution does not exist for the low resolution. The main difference lies in the position of the troughs. For the low resolution the trough to the west and the trough almost in the middle of the channel are approximately 400–500 km farther west compared to their positions using the high resolution. This difference corresponds to a difference in the phase speed of approximately 1 m/sec.

After 10 days there are two well-developed troughs when the high resolution is used, but these can hardly be found when the low resolution is used.

The results of the integration using the fourth-order Scheme J with $\Delta = L/30$ are given in figure 8. The difference between this integration and the integration using Scheme F with $\Delta = L/60$ is very small. After 5 days the amplitudes and the positions of the troughs are almost the same, but after 10 days the trough to the east is farther north and the corresponding jetstream is weaker. However, for these long waves it seems that in the first 10 to 15 days we gain almost the same accuracy by using higher order schemes as by doubling the resolution in a second-order scheme.

The height fields using Scheme H (Shuman's scheme) with $\Delta = L/30$ is given in figure 9. The difference in the

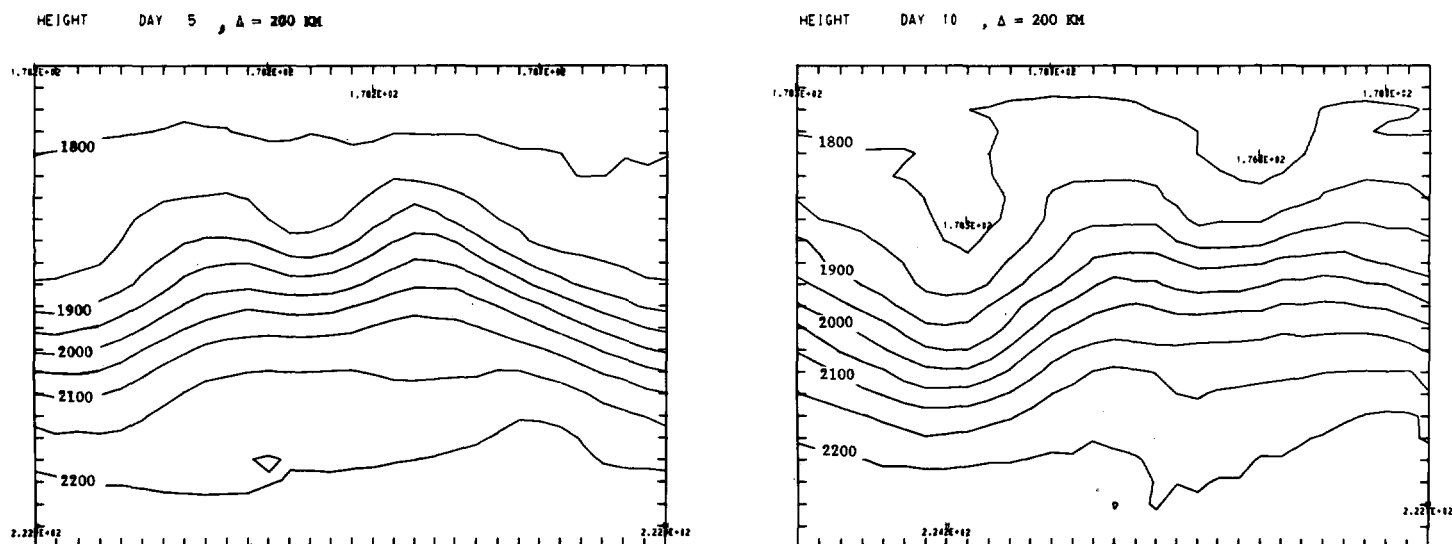


FIGURE 8.—Height fields after 5 and 10 days of integration using the fourth-order Scheme J and Initial Condition I. $\Delta = L/30 = 200$ km. Contours are drawn for every 50 m.

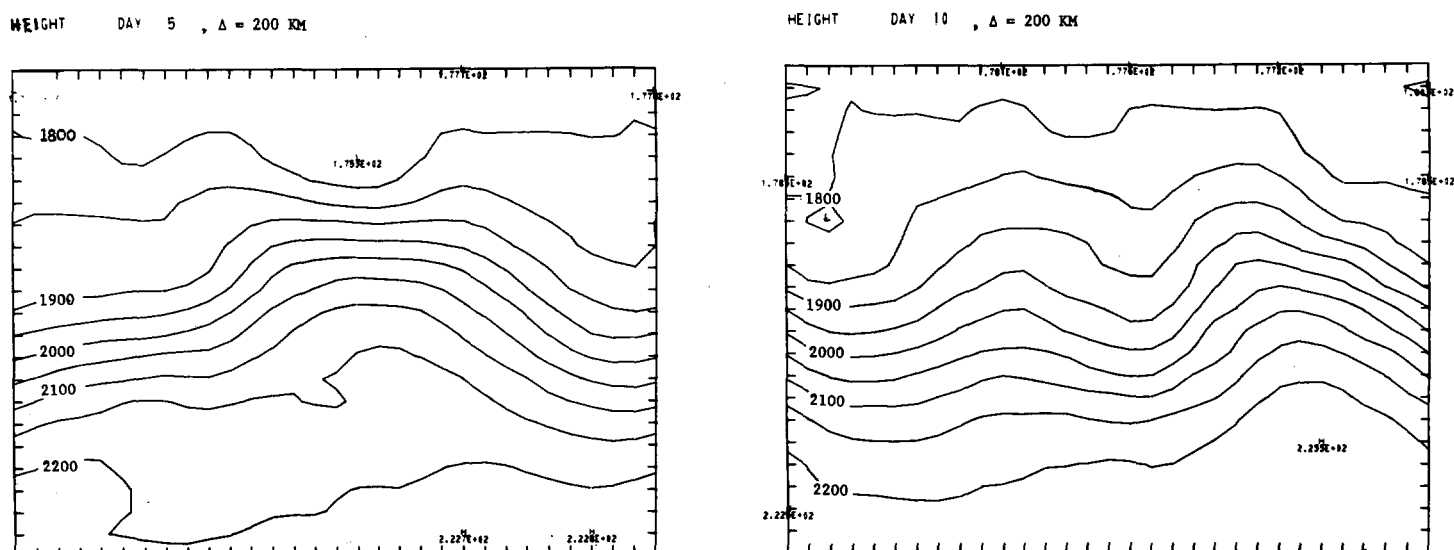


FIGURE 9.—Height fields after 5 and 10 days of integration using Shuman's Scheme H and Initial Condition I. $\Delta = L/30 = 200$ km. Contours are drawn for every 50 m.

amplitudes for the waves between this scheme and Scheme F using $\Delta = L/60$ is not large even after 10 days; but as indicated in section 4, the use of a nine-point formula in space for the derivatives will give larger errors in the phase speeds, and we see that the positions of the troughs are already after 5 days 800–1000 km farther west than the positions of the same troughs for the high resolution in Scheme F. The phase errors are especially large in the space average Schemes G and H, but less for the generalized Arakawa scheme. When high resolution is used in these schemes as well, the phase error becomes smaller, and the solutions for the first 15 days are very similar to the solution for Scheme F.

Figure 10 shows the height fields after 5 days for the fourth-order Scheme J and the generalized Arakawa

Scheme I, using Initial Condition II and the two different grid increments $\Delta = L/30$ and $\Delta = L/60$. For the first 3 days of integrations with the fourth-order scheme, the correlation between the height fields using these two resolutions is relatively large, even if the low resolution does not give wave amplitudes quite as large as the high resolution; already after 5 days, however, we see that the difference between the height fields is very large. In the generalized Arakawa scheme we can still find the three corresponding troughs, but for this scheme as well, the low resolution gives too small amplitudes for the waves.

These integrations indicate that if we are integrating for more than 3 days, we need, even in a fourth-order scheme, more than 10 grid points per wavelength to describe the movement and development of a wave that

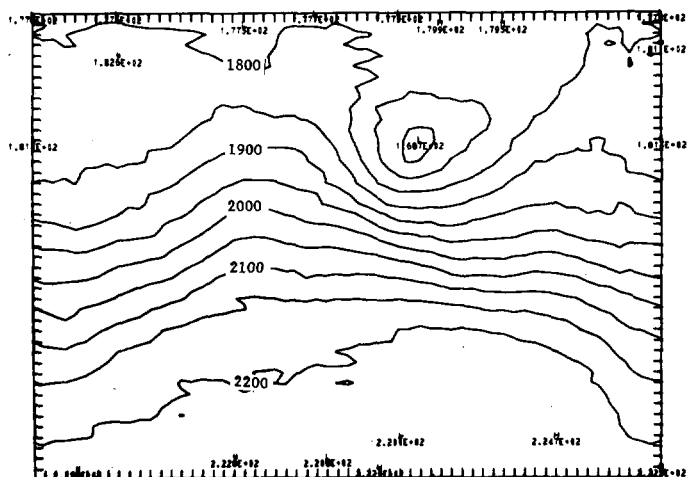
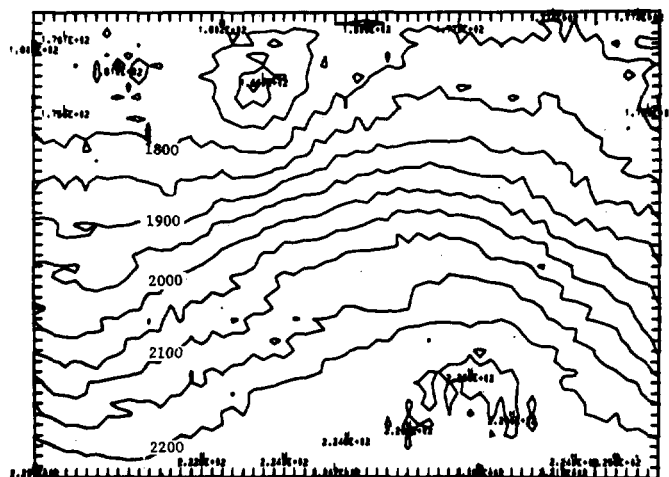
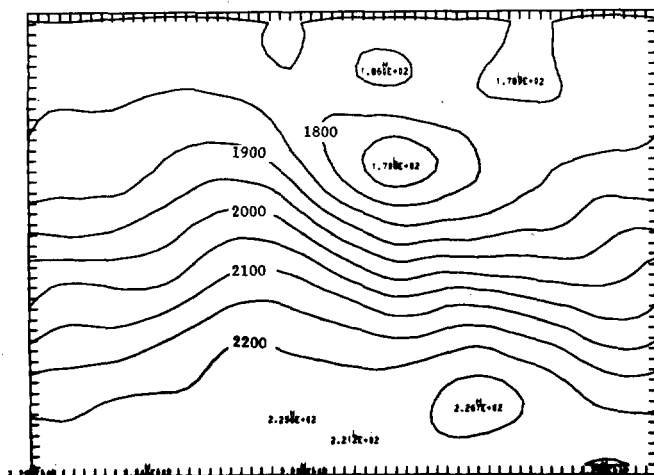
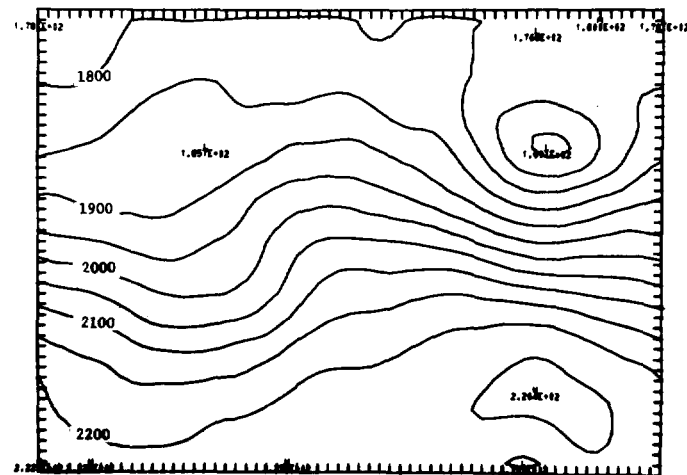
HEIGHT DAY 10, $\Delta = 100$ KMHEIGHT DAY 20, $\Delta = 100$ KMHEIGHT DAY 10, $\Delta = 100$ KMHEIGHT DAY 20, $\Delta = 100$ KM

FIGURE 11.—Height fields after 10 and 20 days of integrations using Initial Condition II and $\Delta = L/60 = 100$ km. Contours are drawn for every 50 m. (Top: the fourth-order Scheme J; bottom: the generalized Arakawa Scheme I.)

more than the slow-moving Rossby waves. But as shown in Appendix 2, these time integration methods will not damp waves with wavelength equal to two grid increments in space. We, therefore, have to add linear viscosity terms to the equations to damp these waves. As shown in figure 12, integrations using a restart with Lax-Wendroff's method each 12 hr and $\nu \geq 3.6 \times 10^3$ m²/sec are stable for more than 20 days. (With the use of $\nu = 3.6 \times 10^2$ m²/sec, the integration became unstable after 9 days.) For $\nu = 3.6 \times 10^3$ m²/sec, the available energy does not decrease more than 4 percent in the first 10 days; but compared to the integrations with Schemes F and J, the amplitudes of the slow-moving Rossby waves are still damped too much even when the high resolution ($\Delta = L/60$) is used.

8. TIME INTEGRATION AND STABILITY

In these experiments the leapfrog method (or the midpoint rule) is used for the time integrations. This

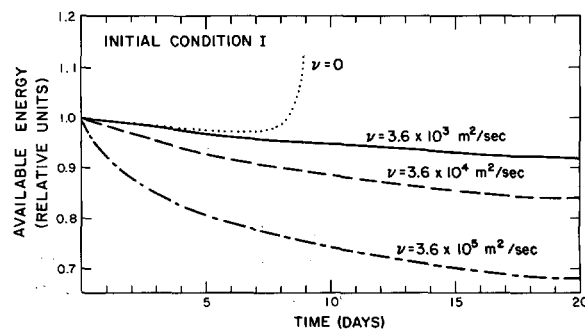


FIGURE 12.—Available energy as a function of time for the time-staggered conservative Scheme D, using Initial Condition I and a restart of the integrations each 12 hr with a two-step Lax-Wendroff method.

is the only commonly used explicit or iterative method, which has no amplification or damping of the solution of the linearized set of equations corresponding to the

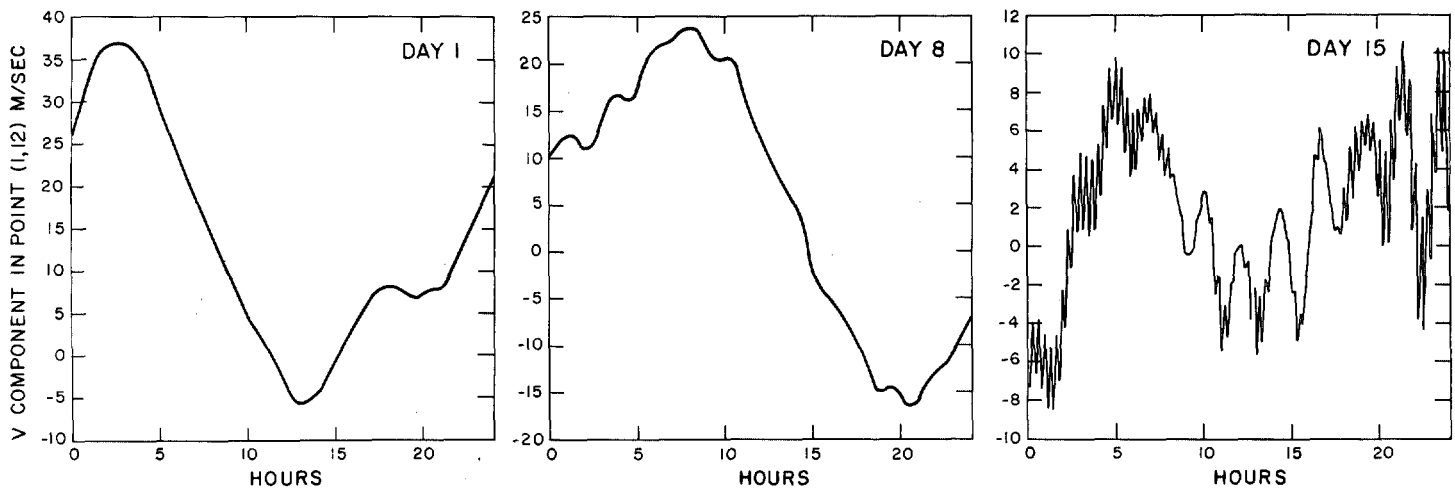


FIGURE 13.—Variation of the meridional velocity component in the point (1.12) with time, using Scheme F and Initial Condition III.

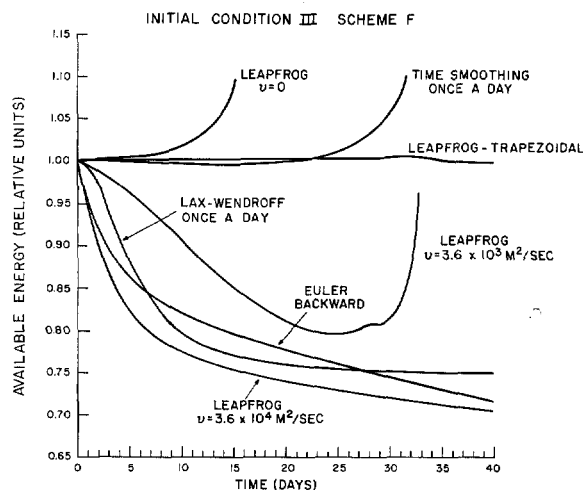


FIGURE 14.—Available energy as a function of time for Scheme F and Initial Condition III using different time integration methods and different eddy viscosity coefficients.

equations (1), (2), and (3) as long as the linear stability condition is fulfilled; but it shares the disadvantages with all multistep methods, that the solution has to be given at more than one time level for each time step, and that the finite-difference equations allow more than one set of solutions. Only one of these sets is physical; the others are computational. In the linear case the amplitude of the computational modes in the leapfrog method may be made small by the starting procedure (Miyakoda, 1962), and since there is no coupling between the different modes they will always remain small thereafter. In the nonlinear case, however, there is a coupling between the different modes, and we have to expect that the amplitude of the computational modes will change when the amplitude of the physical modes change. If we look at the variation in time of the variables at a fixed point, we see that high frequency oscillations are developing; and a few days before the integration becomes unstable, a $2\Delta t$ oscillation is formed, as shown in figure 13

for the v -component in the point (1.12), which is situated in the middle of the channel, using Scheme F and Initial Condition III. From (55) and (62), it follows that the conservation in time of available energy using the leapfrog method also depends on the second derivatives in time of the variables. The stability may therefore be improved by damping the highest frequency oscillations, which in this model are due to the short physical gravity-inertia waves and the computational waves. The short waves may be damped by adding linear viscosity terms to the equation of motion, and the $2\Delta t$ oscillation from the computational waves may be damped by applying a smoothing operator in time for each variable. The smoothing operator

$$\bar{\alpha}_{jk}^r = \alpha_{jk}^r + \frac{(\Delta t)^2}{4} (\alpha_{jk}^r)_{tt}, \quad (75)$$

where α_{jk}^r stands for any variable in the grid point $x=j$, $y=k$ at time $t=r$, will damp the high frequency oscillations and completely remove the $2\Delta t$ oscillation from the integrations if it is used at two sequential time steps.

The energy variation in time, using equation (75) after each day of integration for Scheme F and Initial Condition III, is given in figure 14. We see that the stability increases and the integration becomes unstable after 30 days compared to 16 days without any smoothing.

Other linear, stable multistep time integration methods, which damp the computational modes, and linear stable one-step methods for the linearized set of equations are examined by Kurihara (1965), and we will use two of his methods, the leapfrog-trapezoidal predictor-corrector method and the Euler-backward predictor-corrector method. We will also use the two-step Lax-Wendroff method developed by Richtmyer (1963). These methods are given in Appendix 2.

The leapfrog-trapezoidal method has for the linear equations only weak damping of the physical modes, but strong damping of the computational modes. From figure 14, it

follows that integration with this method for Scheme F and Initial Condition III is more stable than using the leapfrog method with smoothing once a day. For other schemes these two methods give very little difference in the stability and in the time variation of the energy; hence, integrations with the total energy conservative Scheme B seem always to be stable. The computation time for the leapfrog-trapezoidal method is almost twice as long as the computation time for the leapfrog method. Especially for long-term integrations, therefore, it is more economical to use the leapfrog method with an intermittent time smoother than the leapfrog-trapezoidal method.

For the linear equations, the Euler-backward method and the Lax-Wendroff method have the strongest damping of the waves with wavelength equal to four grid increments and little damping of the very long and very short waves; they damp the fast-moving gravity-inertia waves more than the slow-moving Rossby waves. As shown in figure 14 for Scheme F and Initial Condition III, the Euler-backward method gives a decrease in available energy, which corresponds to the use of the leapfrog method with linear viscosity terms, with an eddy viscosity coefficient $\nu \sim 10^4 \text{ m}^2/\text{sec}$ added to the equations of motion. The dissipation of energy using the Lax-Wendroff method is slightly larger than using the Euler-backward method, but as pointed out by Kurihara, the effect of the dissipation may be reduced by using the leapfrog method at most of the time steps and only using the other methods intermittently to damp the gravity-inertia waves. Doing so by restarting the integration after each day using the Lax-Wendroff method still gives a strong damping of the available energy, as shown in figure 14.

9. SUMMARY AND CONCLUSIONS

Ten different finite-difference schemes for the numerical integration of the equations describing barotropic motion in an inviscid, incompressible, hydrostatic fluid with a free surface are tested for stability and accuracy. The integrations show that the quadratic conservative and total energy conservative schemes are more stable than the conservative schemes; but the space average schemes, in which the derivatives in space are calculated over nine grid points, and the generalized Arakawa scheme give the most stable integrations.

The space average schemes and the generalized Arakawa scheme have larger phase errors than the other schemes; they have a smaller growth rate of the small-scale energy and keep the energy on the larger scale for a long time. When the grid increment in the quadratic conservative and total energy conservative schemes is decreased from $\Delta = L/30 \text{ km}$ to $\Delta = L/60 \text{ km}$, the growth rates of the small-scale energy also decrease, and in the first 2 weeks the small-scale energy is little less than the small-scale energy using the space average schemes and the generalized Arakawa scheme with grid increment $\Delta = L/30 \text{ km}$. The decrease in the small-scale energy with decreasing grid incre-

ment indicates that the growth of the small-scale energy is mostly due to the truncation errors and aliasing errors in the schemes.

If the integrations are performed for more than 3 days, we probably need more than 15 grid points per wavelength to describe with any accuracy the movement and development of the shortest wave which initially is carrying a significant part of the energy, and if we integrate for a longer time, we need even higher resolution. Some of the phase errors and the amplitude errors may be reduced by using fourth-order schemes in space. However, fourth-order schemes have larger aliasing errors than second-order schemes, and after a few days when these schemes are used, there is also a rapid increase of small-scale energy.

The conservation of total energy depends also on the second derivative in time of the dependent variables when second-order time integration methods are used. The stability of long-term integrations may therefore be improved by periodically using a smoothing operator in time when a leapfrog method is used, or by using linear stable multistep methods that will damp the highest frequency oscillations in time.

As a rule, linear stable one-step methods have strong built-in dissipation and in a few days will damp out most of the initial perturbation energy, even if they are used only intermittently once a day.

APPENDIX 1

THE GENERALIZED ARAKAWA SCHEME

The finite-difference scheme developed by Arakawa (1966) for the two-dimensional vorticity equation describing frictionless non-divergent flow in a closed domain may be written:

$$\zeta_t + \frac{1}{3} [\bar{\psi}_x \bar{\zeta}_y - \bar{\psi}_y \bar{\zeta}_x + (\bar{\psi}_x^y)_x - (\bar{\psi}_x^x)_y + (\bar{\psi}_y^x)_y - (\bar{\psi}_y^y)_x] = 0 \quad (76)$$

where ψ is the stream function, and $\zeta = \nabla^2 \psi$, and otherwise using the same notation as in section 3. In the closed domain this scheme will conserve the integral of vorticity, kinetic energy, and square of vorticity.

For the equations (1), (2), and (3) describing barotropic frictionless divergent flow with a free surface, we want to derive a finite-difference scheme which reduces to equation (76) when the divergence $\nabla \cdot \mathbf{v} = 0$. To do so we need to rewrite equation (76) in a form using the horizontal velocity components u and v in the x and y direction, respectively, instead of the stream function ψ and the vorticity ζ .

If for the velocity components

$$u = -\frac{\partial \psi}{\partial y} \text{ and } v = \frac{\partial \psi}{\partial x}$$

we use the second-order finite-difference approximations

$$u = -\psi_y \text{ and } v = \psi_x,$$

we see that the problem lies in the form of the second and Jacobian in equation (76). With use of equation (18), this Jacobian may be rewritten as:

$$\begin{aligned} \overline{(\psi_{xy}^v)}_x - \overline{(\psi_{xz}^v)}_y &\equiv 2\overline{(\psi_{xy}^v)}_{xy} - 2\overline{(\psi_{xz}^v)}_{xy} - \overline{(\psi_{xy}^v)}_x + \overline{(\psi_{xz}^v)}_y \\ &\equiv 2\overline{(\psi_{xy}^v)}_{xy} - 2\overline{(\psi_{xz}^v)}_{xy} - \overline{(\psi_{xy}^v)}_x + \overline{(\psi_{xz}^v)}_y, \quad (77) \end{aligned}$$

and in view of equations (11) and (16) as:

$$\begin{aligned} \overline{(\psi_{xy}^v)}_x + \overline{(\psi_{xz}^v)}_y &= -\frac{\Delta^2}{2}(\psi_{xy}^v + \psi_{xz}^v)_x \\ &+ \frac{\Delta^2}{2}(\psi_{xy}^v + \psi_{xz}^v)_y - \overline{(\psi_{xy}^v)}_x + \overline{(\psi_{xz}^v)}_y \\ &= -\frac{\Delta^2}{2}(\psi_{xy}^v)_{xy} + \frac{\Delta^2}{2}(\psi_{xz}^v)_{xy} - \overline{(\psi_{xy}^v)}_x + \overline{(\psi_{xz}^v)}_y. \quad (78) \end{aligned}$$

The first and the last Jacobian in equation (76) may be combined into:

$$\overline{(\psi_{xy}^v)}_x - \overline{(\psi_{xz}^v)}_y - \overline{(\psi_{xy}^v)}_x + \overline{(\psi_{xz}^v)}_y \equiv 2\overline{(\psi_{xy}^v)}_{xy} - 2\overline{(\psi_{xz}^v)}_{xy}. \quad (79)$$

Introducing equations (78) and (79) together with the velocity components u and v into (76) then gives:

$$\begin{aligned} \bar{\zeta}_t + \frac{1}{3} \left\{ 2\overline{(\bar{u}^x \bar{\zeta}^x)}_x + 2\overline{(\bar{v}^y \bar{\zeta}^y)}_y + \frac{\Delta^2}{2}(\bar{u}^x \bar{\zeta}^x)_{xx} + \frac{\Delta^2}{2}(\bar{v}^y \bar{\zeta}^y)_{yy} \right. \\ \left. + \overline{(\bar{u}^y \bar{\zeta}^x)}_x + \overline{(\bar{v}^x \bar{\zeta}^y)}_y \right\} = 0. \quad (80) \end{aligned}$$

The vorticity and the divergence are approximated by:

$$\bar{\zeta} = v_x - u_y \quad (81)$$

and

$$\delta = u_x + v_y = 0. \quad (82)$$

From equations (81) and (82) it follows that

$$\bar{\zeta}_y = v_{xy} - u_{yy} = -(u_{xx} + u_{yy}) = -\nabla^2 u \quad (83)$$

and

$$\bar{\zeta}_x = v_{zx} - u_{yx} = v_{xx} + v_{yy} = \nabla^2 v. \quad (84)$$

Introducing equations (81), (83), and (84) into (80) gives:

$$\begin{aligned} \overline{(\bar{v}_x - \bar{u}_y)}_t + \frac{1}{3} \left\{ 2[\overline{(\bar{u}^x \bar{v}^x)}_x - \overline{(\bar{u}^y \bar{v}^y)}_y] + 2[\overline{(\bar{v}^x \bar{u}^y)}_x - \overline{(\bar{v}^y \bar{u}^x)}_y] \right. \\ \left. + \frac{\Delta^2}{2}(-u \nabla^2 u)_{xy} + \frac{\Delta^2}{2}(v \nabla^2 v)_{xy} + \overline{(\bar{u}^y \bar{v}^x)}_x - \overline{(\bar{u}^x \bar{v}^y)}_y \right\} = 0. \quad (85) \end{aligned}$$

Using equation (16) we see that:

$$-2\overline{(\bar{u}^x \bar{u}^x)}_x - \overline{(\bar{u}^y \bar{u}^y)}_y \equiv -[\overline{(\bar{u}^x \bar{u}^x)}_x + \frac{1}{2}\bar{u}^2_x]_y \quad (86)$$

and

$$2\overline{(\bar{v}^x \bar{v}^x)}_y + \overline{(\bar{v}^y \bar{v}^y)}_x \equiv [\overline{(\bar{v}^x \bar{v}^x)}_y + \frac{1}{2}\bar{v}^2_y]_x, \quad (87)$$

and equation (85) may be written:

$$\begin{aligned} -\{\bar{u}_t + \frac{1}{3}[\overline{(\bar{u}^x \bar{u}^x)}_x + \frac{1}{2}\overline{(u(u + \Delta^2 \nabla^2 u))}_x + 2\overline{(\bar{u}^y \bar{u}^y)}_y + \overline{(\bar{v}^x \bar{u}^y)}_x] \}_y \\ + \{\bar{v}_t + \frac{1}{3}[2\overline{(\bar{u}^x \bar{v}^x)}_x + \overline{(\bar{u}^y \bar{v}^y)}_y + \overline{(\bar{v}^x \bar{v}^x)}_y] \}_x = 0. \quad (88) \end{aligned}$$

To integrate the vorticity equation we may therefore use equations (88) and (82) instead of (76); a finite-difference scheme for the barotropic equations (1), (2), and (3), which is a generalization of Arakawa's scheme for the vorticity equation, is then:

$$\begin{aligned} \bar{u}_t + \frac{1}{3} \{ \overline{(\bar{u}^x \bar{u}^x)}_x + \frac{1}{2} \overline{(u(u + \Delta^2 \nabla^2 u))}_x \\ + 2\overline{(\bar{u}^y \bar{u}^y)}_y + \overline{(\bar{v}^x \bar{u}^y)}_x \} - f\bar{v}^x + \phi_x = 0, \\ \bar{v}_t + \frac{1}{3} \{ 2\overline{(\bar{u}^x \bar{v}^x)}_x + \overline{(\bar{u}^y \bar{v}^y)}_y + \frac{1}{2} \overline{(v(v + \Delta^2 \nabla^2 v))}_y \} + f\bar{u}^x + \phi_y = 0, \quad (89) \end{aligned}$$

and

$$\bar{\phi}_t + (\bar{\phi}^x u)_x + (\bar{\phi}^y v)_y = 0$$

where the location of u , v , and ϕ in the grid are given in figure 3.

APPENDIX 2

TIME INTEGRATION METHODS

In this study four different time integration methods are used: the leapfrog method, the leapfrog-trapezoidal method, the Euler-backward method, and the two-step Lax-Wendroff method. These methods are examined by Kurihara (1965) and by Houghton, Kasahara, and Washington (1966) using the linearized set of equations corresponding to equations (1), (2), and (3). Here we will review some of the characteristics of these methods for these linearized equations.

When the coriolis terms are neglected in the linearized equations, they reduce to three independent equations that formally may be written:

$$\frac{\partial \alpha}{\partial t} + c \frac{\partial \alpha}{\partial x} = 0 \quad (90)$$

where α stands for any of the perturbation quantities $u \pm \phi/\sqrt{gH}$ and v , and c stands for the values $U \pm \sqrt{gH}$ and U . U is the mean zonal velocity, H is the mean height of the free surface, and g is the acceleration of gravity. If the coriolis terms are included, there will be only a small change in the phase speed c and in the linear stability conditions for these methods, except for the Lax-Wendroff method, where the coriolis terms may lead to a weak instability of the solution.

Making equation (90) nondimensional with the same substitutions as in section 2, a solution of (90) for $x=j$ and $t=r$ is:

$$\alpha(j,r) = A e^{i(\theta r + n j)} \quad (91)$$

where n is the wave number and $\theta = -cn$ is the frequency; c is the exact phase speed of the waves. Approximating the space derivative by:

$$\frac{\partial \alpha}{\partial x} \sim \bar{\alpha}_x,$$

and introducing the Fourier term $\alpha(r,j) = \alpha^r e^{in j}$ into equation (90) gives:

$$\frac{\partial \alpha^r}{\partial t} + ic \sin n \alpha^r = 0. \quad (92)$$

Using the four time integration methods, the finite-difference equations for (92) and some of their characteristics are:

Leapfrog method

$$\alpha^{r+1} - \alpha^{r-1} + 2ic \sin n \alpha^r = 0. \quad (93)$$

Introducing

$$\alpha^{r+1} = \omega \alpha^r = \omega^r \alpha^0, \quad (94)$$

where ω is the amplification factor, into (93) gives

$$\omega^2 + 2ic \sin n \omega - 1 = 0. \quad (95)$$

The von Neumann necessary condition for stability is that the magnitude of ω does not exceed unity. The roots of (95) are:

$$\omega_{1,2} = -ic \sin n \pm \sqrt{-c^2 \sin^2 n + 1}, \quad (96)$$

where ω_1 is the amplification factor for the physical mode, and ω_2 is the amplification factor for the computational

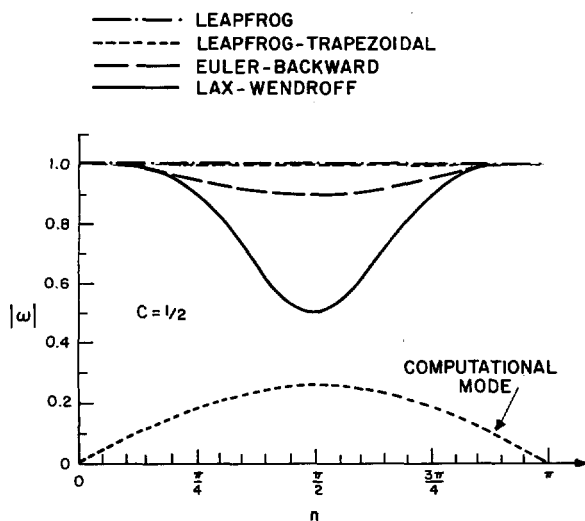


FIGURE 15.—The amplification factor $|\omega|$ for $c = 1/2$ as a function of the wave number n for the different time integration methods.

mode. The magnitudes of $\omega_{1,2}$ are:

$$|\omega_{1,2}| = 1 \quad \text{for } c \leq 1.$$

Leapfrog-trapezoidal method

$$\alpha^* = \alpha^{r-1} - 2ic \sin n \alpha^r$$

and

$$\alpha^{r+1} = \alpha^r - \frac{1}{2}ic \sin n (\alpha^* + \alpha^r). \quad (97)$$

Introducing equation (94) into (97) gives:

$$\omega^2 - [1 - (c \sin n)^2 - \frac{1}{2}ic \sin n] \omega + \frac{1}{2}ic \sin n = 0. \quad (98)$$

The roots of equation (98) are:

$$\omega_{1,2} = \frac{1}{2} [1 - (c \sin n)^2 - \frac{1}{2}ic \sin n] \pm \frac{1}{2} \sqrt{[1 - (c \sin n)^2 - \frac{1}{2}ic \sin n]^2 - 2ic \sin n}, \quad (99)$$

and the magnitudes of the amplification factors are:

$$|\omega_{1,2}| \leq 1 \quad \text{for } c \leq \sqrt{2}.$$

Euler-backward method

$$\alpha^* = (1 - ic \sin n) \alpha^r$$

$$\alpha^{r+1} = \alpha^r - ic \sin n \alpha^* \quad (100)$$

or

$$\alpha^{r+1} = \omega \alpha^r,$$

where the amplification factor ω is:

$$\omega = 1 - (c \sin n)^2 - ic \sin n. \quad (101)$$

The magnitude of ω becomes:

$$|\omega|^2 = 1 - (c \sin n)^2 + (c \sin n)^4 \quad (102)$$

and

$$|\omega|^2 \leq 1 \quad \text{for } c \leq 1.$$

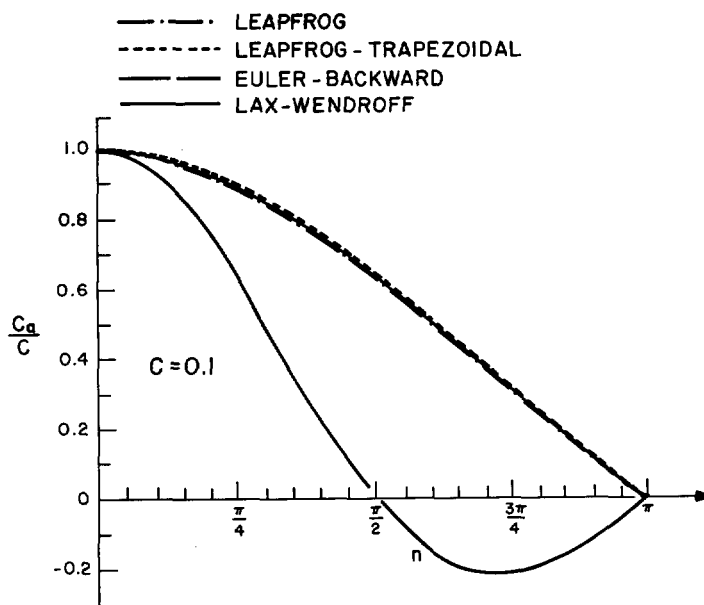


FIGURE 16.—Ratio of the approximated phase speed to the true value of the phase speed for $c = 0.1$ as a function of the wave number n for the different time integration methods.

Two-step Lax-Wendroff method

$$\alpha^{r+1} = (\cos n - ic \sin n) \alpha^r$$

and

$$\alpha^{r+2} = \alpha^r - 2ic \sin n \alpha^{r+1} \quad (103)$$

or

$$\alpha^{r+2} = \omega \alpha^r$$

where

$$\omega = 1 - 2c \sin^2 n - 2ic \sin n \cos n. \quad (104)$$

The magnitude of ω is given by:

$$|\omega|^2 = 1 - 4c^2 (1 - c^2) \sin^2 n \quad (105)$$

and

$$|\omega|^2 \leq 1 \quad \text{for } c \leq 1.$$

Except for the leapfrog method, which has no damping of the amplitudes of the waves, it follows from equations (99), (102), and (105) that the damping of the amplitudes using the other methods is largest for wave number $n = \pi/2$, and there is no damping for $n = 0$ and $n = \pi$. $n = \pi$ corresponds to a wave with a wavelength of two grid increments, and we may, therefore, expect that the short waves may grow and eventually dominate the solutions when these methods are used in numerical integrations of nonlinear equations.

The amplification factor $|\omega|$ for $c = 1/2$ is given in figure 15. We see that the leapfrog-trapezoidal method has a strong damping of the computational mode but only weak damping of the physical mode. The Euler-backward method damps the wave with wavelength of four grid increments ($n = \pi/2$) almost 10 percent for each timestep, and the two-step Lax-Wendroff method damps the same wave 50 percent, but after two time steps. When c is larger, the damping of the physical mode is also larger, but the damping of the computational mode in the leapfrog-trapezoidal method is smaller.

The approximated phase speeds of the waves for the different methods may be found from equations (96), (99), (101), and (104), and in figure 16 is given the ratio of the approximated phase speeds c_a to the true value of the phase speed c for $c = 1$. The errors in the phase speeds for the leapfrog method, the leapfrog-trapezoidal method, and the Euler-backward method are almost the same, and we see that the errors in the phase speeds are more than 10 percent for waves with wavelength less than eight grid increments ($n = \pi/4$). For the two-step Lax-Wendroff method, the errors in the phase speeds are even larger, and the phase speeds become negative for the short waves ($\pi/2 < n < \pi$) and will therefore change sign each two time steps for these waves.

ACKNOWLEDGMENTS

The author wishes to thank Dr. A. Kasahara and Dr. W. Washington for their careful reading and valuable criticism of the manuscript. Thanks are also due Mr. Ronald Cox for editorial assistance in preparing the article, and to Miss Susan Farrell for typing the manuscript.

REFERENCES

- Arakawa, A., "Computational Design for Long-Term Numerical Integration of the Equations of Fluid Motion: I. Two-Dimensional Incompressible Flow," *Journal of Computational Physics*, Vol. 1, No. 1, Academic Press, New York, Aug. 1966, pp. 119-143.
- Bryan, K., "A Numerical Investigation of a Nonlinear Model of a Wind-Driven Ocean," *Journal of Atmospheric Sciences*, Vol. 20, No. 6, Nov. 1963, pp. 594-606.
- Bryan, K., "A Scheme for Numerical Integration of the Equations of Motion on an Irregular Grid Free of Nonlinear Instability," *Monthly Weather Review*, Vol. 94, No. 1, Jan. 1966, pp. 39-40.
- Eliassen, A., Grammelvedt, A., and Bremnes, O., "Studies in Numerical Weather Prediction," *Final Report*, Contract AF 61(052)-525, Institutt for Teoretisk Meteorologi, University of Oslo, Aug. 1964, 67 pp.
- Gates, W. L., "A Numerical Study of Transient Rossby Waves in a Wind-Driven Homogeneous Ocean," *Journal of Atmospheric Sciences*, Vol. 25, No. 1, Jan. 1968, pp. 3-22.
- Grimmer, M., and Shaw, D. B., "Energy-Preserving Integrations of the Primitive Equations on the Sphere," *Quarterly Journal of the Royal Meteorological Society*, Vol. 93, No. 397, July 1967, pp. 337-349.
- Houghton, D., Kasahara, A., and Washington, W., "Long-Term Integration of the Barotropic Equations by the Lax-Wendroff Method," *Monthly Weather Review*, Vol. 94, No. 3, Mar. 1966, pp. 141-150.
- Jelesnianski, C. P., "Numerical Computations of Storm Surges With Bottom Stress," *Monthly Weather Review*, Vol. 95, No. 11, Nov. 1967, pp. 740-756.
- Kurihara, Y., "On the Use of Implicit and Iterative Methods for the Time Integration of the Wave Equation," *Monthly Weather Review*, Vol. 93, No. 1, Jan. 1965, pp. 33-46.
- Kurihara, Y., and Holloway, J. L., Jr., "Numerical Integration of a Nine-Level Global Primitive Equations Model Formulated by the Box Method," *Monthly Weather Review*, Vol. 95, No. 8, Aug. 1967, pp. 509-530.
- Lax, P. D., and Wendroff, B., "System of Conservation Laws," *Communications on Pure and Applied Mathematics*, Vol. 13, No. 2, Interscience Publishers, Inc., New York, May 1960, pp. 217-237.
- Lilly, D. K., "On the Computational Stability of Numerical Solutions of Time-Dependent Non-Linear Geophysical Fluid Dynamic Problems," *Monthly Weather Review*, Vol. 93, No. 1, Jan. 1965, pp. 11-26.
- Matsuno, T., "Numerical Integrations of the Primitive Equations by a Simulated Backward Difference Method," *Journal of the Meteorological Society of Japan*, Ser. 2, Vol. 44, No. 1, Feb. 1966, pp. 76-84.
- Miyakoda, K., "Contribution to the Numerical Weather Prediction: Computation With Finite Difference," *Japanese Journal of Geophysics*, Vol. 3, No. 1, Mar. 1962, pp. 75-190.
- Phillips, N. A., "An Example of Non-Linear Computational Instability," *The Atmosphere and Sea in Motion*, Rockefeller Institute Press, New York, 1959, pp. 501-504.
- Richtmyer, R. D., "A Survey of Difference Methods for Non-Steady Fluid Dynamics," *NCAR Technical Notes*, 63-2, National Center for Atmospheric Research, Boulder, Colo., 1963, 25 pp.
- Shuman, F. G., "Numerical Experiments With the Primitive Equations," *Proceedings of the International Symposium on Numerical Weather Prediction in Tokyo, November 1960*, Meteorological Society of Japan, Tokyo, Mar. 1962, pp. 85-107.
- Shuman, F. G., and Vanderman, L. W., "Difference System and Boundary Conditions for the Primitive-Equation Barotropic Forecast," *Monthly Weather Review*, Vol. 94, No. 5, May 1966, pp. 329-335.
- Smagorinsky, J., Manabe, S., and Holloway, J. L., Jr., "Numerical Results From a Nine-Level General Circulation Model of the Atmosphere," *Monthly Weather Review*, Vol. 93, No. 12, Dec. 1965, pp. 727-768.
- von Neumann, J., and Richtmyer, R. D., "A Method for the Numerical Calculation of Hydrodynamic Shocks," *Journal of Applied Physics*, Vol. 21, No. 3, Mar. 1950, pp. 232-237.